The chemistry and saturation states of subsurface fluids during the in situ mineralisation of CO_2 and H_2S at the CarbFix site in SW-Iceland

Sandra Ó. Snæbjörnsdóttir

Institute of Earth Sciences

University of Iceland

Askja

Sturlugata 7

101 Reykjavík, Iceland

tel. 354-525-5414

fax. 354-525-4499

sos22@hi.is

The chemistry and saturation states of subsurface fluids during the *in situ* mineralisation of CO_2 and H_2S at the CarbFix site in SW-Iceland

Sandra Ó. Snæbjörnsdóttir[1], Eric H. Oelkers[1,2,3], Kiflom Mesfin[1], Edda Sif Aradóttir[4], Knud Dideriksen[5], Ingvi Gunnarsson[4], Einar Gunnlaugsson[4], Juerg M. Matter[6,7], Martin Stute[7], Sigurdur R. Gislason[1]

[1]*Institute of Earth Science, University of Iceland, Iceland*
[2]*CNRS/UMR 5563, Université Paul Sabatier, France*
[3]*Earth Science, University College London, UK*
[4]*Reykjavik Energy, Iceland*
[5]*Nano-Science Center, Department of Chemistry, University of Copenhagen, Denmark*
[6]*Ocean and Earth Science, University of Southampton, UK*
[7]*Lamont-Doherty Earth Observatory, Columbia University, USA*

Abstract

In situ carbonation of basaltic rocks could provide a long-term carbon storage solution, which is essential for the success and public acceptance of carbon storage. To demonstrate the viability of this carbon storage solution, 175 tonnes of pure CO_2 and 73 tonnes of a 75% CO_2-24% H_2S-1% H_2-gas mixture were sequentially injected into basaltic rocks at the CarbFix site at Hellisheidi, SW-Iceland from January to August 2102. This paper reports the chemistry and saturation states with respect to potential secondary minerals of sub-surface fluids sampled prior to, during, and after the injections. All gases were dissolved in water during their injection into permeable basalts located at 500-800 m depth with temperatures ranging from 20 to 50°C. A pH decrease and dissolved inorganic carbon (DIC) increase was observed in the first monitoring well, HN-04, about two weeks after each injection began. At storage reservoir target depth, this diverted monitoring well is located ~125 m downstream from the injection well. A significant increase in H_2S concentration, however, was not observed after the second injection. Sampled fluids from the HN-04 well show a rapid increase in Ca, Mg, and Fe concentration during the injections with

a gradual decline in the following months. Calculations indicate that the sampled fluids are saturated with respect to siderite about four weeks after the injections began, and these fluids attained calcite saturation about three months after each injection. Pyrite is supersaturated prior to and during the mixed gas injection and in the following months. In July 2013, the HN-04 fluid sampling pump broke down due to calcite precipitation, verifying the carbonation of the injected CO_2. Mass balance calculations, based on the recovery of non-reactive tracers co-injected into the subsurface together with the acid-gases, confirm that more than 95% of the CO_2 injected into the subsurface was mineralised within a year, and essentially all of the injected H_2S was mineralised within four months of its injection. These results demonstrate the viability of the *in situ* mineralisation of these gases in basaltic rocks as a long-term and safe storage solution for CO_2 and H_2S.

Introduction

Attenuating the current increasing atmospheric CO_2 concentration is one of the greatest challenges of this century (e.g. Broecker, 2007; Broecker and Kunzig, 2008; Global CCS Institute, 2015; Hoffert et al., 2002; International Energy Agency, 2015 ; IPCC, 2005, 2014; Lackner, 2003; Oelkers and Schott, 2005; Oelkers and Cole, 2008; Pacala and Socolow, 2004). One potential solution to this challenge is carbon capture and storage (CCS). A critical step in CCS is identifying locations and methods for secure subsurface CO_2 storage.

This paper follows two previous reports on the CarbFix injection, 1) a detailed description of the injection method and data from the injection well was presented by Sigfússon et al. (2015) and 2) the monitoring of tracers, carbon and pH in the first monitoring well downstream from the injection well was reported by Matter et al. (2016). The CarbFix project is focussed on CO_2 and H_2S injected into basaltic rocks. Carbon storage in basaltic rocks offers several advantages, due to their ability to promote permanent CO_2 storage by mineralisation and due to their large potential storage volume (Gislason and Oelkers, 2014; Goldberg and Slagle, 2009; Goldberg et al., 2010; McGrail et al., 2006; Snæbjörnsdóttir et al., 2014). As such, a large number of past studies have focussed on developing the technology to safely store CO_2 in basaltic rocks (Assayag et al., 2009; Bacon et al., 2014; Flaathen et al., 2009; Galeczka et al., 2014; Goldberg et al., 2013; Goldberg et al., 2008; Gudbrandsson et al., 2011; Gysi and Stefánsson, 2012a; Matter et al., 2007; McGrail et

al., 2012; McGrail et al., 2006; McGrail et al., 2011; Rogers et al., 2006; Rosenbauer et al., 2012; Sigfusson et al., 2015; Stockmann et al., 2011; Van Pham et al., 2012). Basaltic rocks are rich in divalent cations such as Ca^{2+}, Mg^{2+}, and Fe^{2+}. Acidic gas-charged water accelerates the release of these metals, promoting the formation of carbonate minerals such as calcite, magnesite, and siderite (Gislason et al., 2014; Gislason and Oelkers, 2014; Olsson et al., 2014; Gislason et al., 2010; Gunnarsson et al., 2011; Oelkers et al., 2008; Stefánsson et al., 2011). About 10% of the continents and most of the oceanic floor are comprised of basaltic rocks, including the mid-oceanic ridges. The largest basaltic storage potential lies offshore; theoretically all CO_2 from the burning of fossil fuel carbon (~5000 GtC; Archer, 2005) could be stored by mineral carbonation along the mid-ocean ridges (Snæbjörnsdóttir et al., 2014). The flanks of the ridges contain highly fractured and permeable basaltic layers (Fisher, 1998) with a pervasive circulation of about 1,000 Gt seawater/yr (Harris and Chapman, 2004). The potential for using these systems for carbon storage is confirmed by the results of Wolff-Boenisch et al. (2011), who demonstrated the rapid dissolution basaltic rocks in CO_2 charged seawater.

About 90% of Icelandic bedrock is basaltic (Hjartarson and Sæmundsson, 2014). In total, Iceland produced 1.6 $MtCO_2$ by industrial processes in 2012 and about 0.2 $MtCO_2$ by geothermal energy production (Wöll et al., 2014). Iceland is the largest (103,000 km^2) part of the mid-ocean ridge systems exposed above sea level. Iceland, therefore, provides an excellent opportunity to explore the feasibility of mineral storage of CO_2 and gas mixtures in basaltic rocks at the oceanic ridges since drilling and detailed monitoring of injected gas and water by reactive and non-reactive tracers is much less costly onshore than offshore.

The potential advantages in storing carbon by the *in situ* carbonation of Icelandic basalts motivated creation of the CarbFix project, which was designed to inject CO_2 into subsurface adjacent to the Hellisheidi geothermal power plant. Extensive research was carried out prior to the injection of acid gases at the CarbFix site. Gislason et al. (2010) described the thermodynamics and kinetic basis for carbon storage at this site. Alfredsson et al., (2013) characterised the geology, and rock and water chemistry of the CarbFix site. Wiese et al. (2008) determined the amount and spatial distribution of naturally mineralised CO_2 within the Icelandic geothermal systems. The dissolution and precipitation rates of the subsurface rocks at the site were investigated in mixed

93 flow reactors (e.g. Gudbrandsson et al., 2011; Gysi and Stefánsson, 2012a; Stockmann et al.,
94 2013), in pressurised plug flow experiments (e.g. Galeczka et al., 2014), by hydrological modelling
95 (Khalilabad et al., 2008), and using reactive transport modelling (Aradóttir et al., 2012).
96
97 The CarbFix project is unique in that it injects CO_2 into basalts as a dissolved aqueous
98 phase. In contrast, most subsurface carbon storage projects have injected CO_2 as a separate phase
99 into large sedimentary basins; this method requires high integrity cap-rocks to keep the injected
100 buoyant gas in the subsurface (Gislason and Oelkers, 2014; Rutqvist et al., 2007). However, there
101 are numerous advantages of injecting CO_2 into the subsurface within an aqueous phase. First,
102 many of the risks associated with buoyancy can be mitigated by dissolving the gases into water
103 during their injection (Gislason et al., 2010; Sigfusson et al., 2015). Once dissolved, the injected
104 gases are no longer buoyant, making it possible to inject CO_2 into fractured rocks, such as basalts
105 along the ocean ridges and on the continents. Furthermore, this injection method may also make it
106 possible to simultaneously store a number of acid gases including SO_2 and H_2S as sulphide
107 minerals such as pyrite and pyrrhotite, lowering substantially gas capture/storage costs (Gislason et
108 al., 2014; Gislason and Oelkers, 2014; WorleyParsons and Schlumberger, 2011).
109
110 Large SO_2 emissions are associated with fossil fuel power production and heavy industry
111 such as metal smelters (Smith et al., 2011). These emissions peaked in 1970-1980 at about 80 Mt
112 per year in the USA and Europe leading to acid rain and Al mobilisation, degrading aquatic and
113 terrestrial ecosystems (Gensemer and Playle, 1999; Gislason and Torssander, 2006). Due to
114 intervening regulations, these emissions have been in decline, and were less than 11 Mt in 2011
115 (European Environment Agency, 2014; United States Environmental Protection Agency, 2015)
116 due, in large part due to SO_2 capture. This SO_2 capture could potentially be combined with CO_2
117 capture in water, and this water-soluble gas mixture injected into reactive rocks for mineral
118 storage.
119
120 Emissions of H_2S are an inevitable consequence of geothermal energy exploitation, pulp
121 and paper production and the use of fossil fuels (e.g.World Health Organization, 2000).
122 Regulations for H_2S emissions have obliged Icelandic geothermal energy producers to reduce their
123 emissions of this gas (Aradóttir et al., 2015; Gunnarsson et al., 2011). One mitigation option is to

capture H_2S and inject it into the subsurface. This approach has been adopted by an ongoing carbon storage project at Weyburn Canada in connection with enhanced oil recovery, which has been co-injecting supercritical CO_2 and H_2S into subsurface sedimentary rocks (Bachu and Gunter, 2005). The behaviour of co-injecting H_2S has not been studied to the same extent as injection of pure CO_2. Some work has, however, been done in terms of geochemical modelling and laboratory experiments (e.g. Bacon et al., 2014; Gudbrandsson and Stefánsson, 2014; Gunnarsson et al., 2011; Stefánsson et al., 2011; Knauss et al., 2005). One goal of the CarbFix project is to assess the feasibility of co-injecting dissolved H_2S and CO_2 into basalts which can provide a cost effective storage solution for both of these gases.

This paper reports on our further efforts to develop the technology to store CO_2 through the *in situ* carbonation of basaltic rocks at the CarbFix storage site in southwest Iceland. Two field injections were carried out at this storage site. In January to March 2012, 175 tonnes of pure CO_2 were injected into the CarbFix site. In June to August 2012, 73 tonnes of a gas mixture from the Hellisheidi geothermal power plant were injected, consisting of 75 mol% CO_2, 24 mol% H_2S and 1 mol% H_2. In each case, the gases were dissolved into formation water during their injection, releasing a single aqueous fluid into the storage formation. Here we report the compositions and saturation states of fluid samples collected from a diverted monitoring well located 125 m in the down-flow direction of the injection well at target storage reservoir depth, before, during, and after the CO_2 and CO_2-H_2S injections, and use these results to better understand the fate of these injected gases in the subsurface.

Methods

Description of the CarbFix site

The CarbFix injection site is located in SW-Iceland, about 30 km east of Reykjavík. The site is ~260 m above sea level and located 3 km SW of the Hellisheidi geothermal power plant (Fig. 1), which is owned and operated by Reykjavik Energy. During 2015, the power plant generated 303 MW of electricity and 133 MW of thermal energy using hot water and steam from a high temperature reservoir located at 800-3000 m depth E and NE of the power plant. The

power plant annually produces 40,000 tonnes CO_2 and 12,000 tonnes H_2S. These gases are of magmatic origin produced as a by-product of the geothermal energy production.

Acidic gases injected at the CarbFix site were dissolved into water collected from HN-01, a well located about 1 km west of the 2001 m deep HN-02 injection well (Fig. 1). Well HN-01 is 1306 m deep; water collected from this well was transported via pipeline to HN-02 where the HN-01 water was injected through a pipe as described in detail by Sigfusson et al. (2015). The injected gas was released into the down flowing water via a sparger at a depth of 340 m. The gas dissolved in the water as it was carried down a mixing pipe to a depth of 540 m, where the hydrostatic pressure is above 40 bars, ensuring complete dissolution of the CO_2 before it was released into the subsurface rocks (Aradóttir et al., 2012; Gislason et al., 2010; Sigfusson et al., 2015).

The geology of the CarbFix site was described in detail by Alfredsson et al. (2013). The subsurface rocks at the injection site are primarily olivine tholeiite basalts, consisting of post-glacial lava flows and glassy hyaloclastite formations, formed beneath the ice-sheet during glaciations (Fig. 1). The bedrock down to about 200-300 m depth consists of relatively unaltered olivine tholeiite lava flows that host an oxygen-rich groundwater system with a static water table at about 100 m depth. Below the lava flows lies a 200 m thick, slightly altered hyaloclastite that separates the near surface water system from a deeper system, which is oxygen depleted. The site follows an approximately linear temperature gradient of 80°C/km. The target injection formation consists of a series of altered lava flows from about 400 m to 800 m depth overlain by the low permeability hyaloclastites (Alfredsson et al., 2013; Helgadóttir, 2011). The lateral and vertical intrinsic permeabilities of the storage formation were estimated to be 300 and 1700 x 10^{-15} m^2, respectively, having an effective matrix porosity of 8.5% and a 25 m/year estimated regional groundwater flow velocity (Aradóttir et al., 2012). The most abundant alteration minerals from 200 m to 1000 m depth are smectites, calcite, and Ca- and Na-rich zeolites (Alfredsson et al., 2013; Helgadóttir, 2011).

The injection site is equipped with eight monitoring wells ranging from 50 to 1300 m depth. Six of the eight wells are located downstream from the HN-02 injection well. Four of the

wells penetrate the groundwater system in the topmost 200-300 m and four are drilled down through the target storage formation. These deeper wells are cased down to 400 m depth and serve as monitoring wells of the deeper system. All monitoring wells were sampled during the experiment, but evidence of tracers from the injections has only been found, to date, in samples collected from well HN-04, which is the closest to the injection well as shown in Figure 1. Well HN-04 is located about 10 m west of HN-02 at the surface, but it is diverted in the subsurface such that the distance between the wells is 125 m at 520 m depth, where the target carbon storage aquifer is located (Alfredsson et al., 2013; Aradóttir et al., 2012). Field injections at the CarbFix site were performed from 2008 to 2012. Tracer tests were conducted both under natural and forced flow conditions from 2008 to 2011 to define the system hydrology and for scaling reactive transport models (Aradóttir et al., 2012; Gislason et al., 2010; Khalilabad et al., 2008; Matter et al., 2011).

Acid Gas Injections at the CarbFix site

The injection of acid gases at the CarbFix site was performed in two phases during 2012 (Table 1):

Phase I began in late January 2012 with the injection of 175 tonnes of pure CO_2. The CO_2 was stored in a 30 m^3 reservoir tank pressurised at 26-28 bars and co-injected with water collected from well HN-01 into well HN-02, as described by Sigfusson et al. (2015). The predicted *in situ* pH and DIC concentrations of the injected fluid during Phase I were 3.85 and 0.823 mol kg^{-1} respectively, based on the mass flow rates of water and gas into the injection well, chemical speciation calculations (Parkhurst and Appelo, 2013), and direct measurement (Sigfusson et al., 2015). The chemical tracers listed in Table 1 were co-dissolved into the injected water as described by Sigfusson et al. (2015) to aid in determining the fate of the dissolved CO_2 as described by Matter et al. (2016). The Phase I injection ran continuously until it was terminated on the 9th of March 2012.

Phase II began in mid-June 2012 with the injection of 73 tonnes of a gas mixture containing 75 mol% CO_2, 24 mol% H_2S, and 1 mol% H_2 originating from the Hellisheidi power plant. The gas mixture was obtained by diverting power plant emissions to a gas abatement plant, where it was

separated into water soluble gases (CO_2, H_2S), and less soluble gases (N_2, CH_4, H_2, Ar). The power plant emission gas contained about 20% H_2; a small fraction of this dissolves in the water along with the CO_2 and H_2S according to the solubility and partial pressure of the gases. Subsequently the soluble gas mixture was co-injected into the surface with HN-01 water. The predicted *in situ* pH, DIC, H_2S, and H_2 concentrations of the injected water during the Phase II, based on the mass flow rates of water and gas into the injection well and chemical speciation calculations performed using PHREEQC (Parkhurst and Appelo, 2013) were 4.03, 0.43 mol kg^{-1}, 0.14 mol kg^{-1} and less than 0.01 mol kg^{-1}, respectively. The chemical tracers listed in Table 1 were co-dissolved into the injected water as for the pure CO_2 injection to monitor subsurface reactivity. The gas mixture injection rate was less stable than that of the pure CO_2 injection and was stopped several times due to injection problems. The injection was terminated on the 1st of August 2012.

Analytical methods

Sampling of the fluids from the HN-04 first monitoring well began in 2008. Water samples for chemical analysis were collected several times prior to the Phase I injection in January 2012 (Alfredsson et al., 2013). During the injections and until mid-September 2012 this well was sampled twice weekly. Weekly sampling continued until mid-July 2013 with few exceptions.

Water was pumped from the monitoring well at the rate of 3.5 m^3/h throughout this study, to maintain a constant head from the injection to the monitoring well. The pump used was a 163 cm long, submersible Grundfos model SP3A-60 made of stainless steel, located at 303 m depth and ~200 m below the water table. This pump was connected to a 53 mm diameter steel pipe to the surface where the effluent was deposed via a service pipe extending east of the injection site and eventually re-injected into a deep geothermal system.

Fluid samples were collected via a 10 m long, 10 mm diameter stainless steel pipe connected to the 53 mm diameter monitoring well lining pipe extending down to the pump. The 10 mm sample pipe was connected directly to a sampling valve inside an on-site field laboratory. After flushing the sampling pipe, the sampled waters were immediately filtered through 0.2 µm

Millipore cellulose acetate membranes using silicon tubing and a 140 mm Sartorius® polypropylene filter holder. All air in the filtration system was expelled through a valve prior to sampling and at least 3 L of water was pumped through the system before the samples were collected in distinct bottles depending on the subsequent chemical analysis. Amber glass bottles were used to collect samples for pH and alkalinity. Acid washed high density polyethylene bottles were used to collect samples for cations and trace metals. These samples were acidified using Suprapur® HNO_3, 1% (v/v). Acid washed low density polypropylene bottles were used to collect samples for Fe-species measurement. These samples were acidified with Suprapur® HCl, 1% (v/v) immediately after collection. Low density polypropylene bottles were used for collecting samples for anion concentration measurements. Acid washed polycarbonate bottles were used to collect samples for dissolved organic carbon (DOC). These samples were acidified with 1.2 M concentrated HCl 2% (v/v). All sample bottles were rinsed three times by half filling them with the filtrated water and then emptying them prior to sample collection.

Temperature and conductivity were measured at the sampling site using a Eutech Instruments Oakalon 2-cell Conductivity meter. The *in situ* temperature of the sampled fluid was determined using down-hole temperature logging at the depth of the main feed-point of well HN-04, at about 420 m depth (Alfredsson et al., 2013; Thorarinsson et al., 2006). The pH was determined on site with a Eutech InstrumentsTM CyberScan pH 110 electrode and again in the laboratory a few hours after sampling with a Cole Parmer combined glass electrode together with an Orion pH meter. The uncertainty of the analyses is estimated to be ±0.02. The pH was then re-calculated at *in situ* conditions using PHREEQC (Parkhurst and Appelo, 2013). Alkalinity was measured in the laboratory by alkalinity titration using the Gran function to determine the end point of the titration (Stumm and Morgan, 1996). Total dissolved inorganic carbon (DIC) was calculated with PHREEQC (Parkhurst and Appelo, 2013) using measured pH, alkalinity, temperature and total dissolved elements concentrations. The uncertainties of the DIC calculations are estimated to be within 10%.

Dissolved oxygen was fixed on site and later determined by Winkler titration. This method has a precision of 1 µmol/L O_2 (0.03 ppm) for the 50 ml sample bottles, but there is a risk of atmospheric contamination for samples containing no or little oxygen. Such is the case for

278 the samples collected from HN-04, which are oxygen depleted. The O_2 concentrations of the
279 sampled fluids ranged from 2-24 µmol/L. The difference between the O_2 concentration in the
280 samples and the reagents was determined using the method described by Arnórsson (2000). The
281 results show that the oxygen measured in the samples is mostly derived from the reagents. Some
282 oxygen contamination during sampling was also inevitable.
283
284 Dissolved hydrogen sulphide was measured by titration on site using mercury and
285 dithizone as an indicator (Arnórsson et al., 2000). The sensitivity of this method is about 0.29
286 µmol/L H_2S (about 0.01 ppm) when using a 50 ml sample aliquot.
287
288 The major elements Si, Ca, K, Mg, Na, and S and the trace metals Fe and Al were
289 analysed using a Spectro Ciros Vision Inductively Coupled Plasma Optical Emission
290 Spectrometer (ICP-OES) using an in-house multi-elements standard checked against the SPEX
291 Certified Reference standard at the University of Iceland. The samples were analysed again using
292 a Agilent 725 ICP-OES for major elements and an ELEMENT XR Inductively Coupled Plasma
293 Sector Field Mass Spectrometer (ICP-SFMS) from ThermoScientific for the trace elements Fe
294 and Al at ALS Scandinavia, Luleå, Sweden. Analytical measurements for the major elements had
295 an inter-laboratory reproducibility within 12%. The average difference between corresponding
296 concentration measurements is 3.7% with a standard deviation of 2.3%. Analytical
297 measurements for the trace elements Fe and Al had an inter-laboratory reproducibility within
298 19%. The average difference in corresponding Fe and Al concentration measurements was 4.9%.
299 Dissolved F^-, Cl^-, and SO_4^{-2} concentrations were quantified using a DIONEX, ICS-2000 Ion
300 Chromatograph. The addition of zinc-acetate to the SO_4 sample was not needed for its analysis
301 since the H_2S concentrations were small compared to the SO_4 concentrations as shown below.
302 Concentrations of Fe^{2+} and Fe^{3+} were measured using a DIONEX IC-3000 Ion Chromatograph.
303 Due to ambiguities in the Fe^{3+} measurements, the Fe^{2+} measurements were used along with the
304 Fe_{total} concentrations measured by ICP-SFMS at ALS Scandinavia to calculate Fe^{3+}
305 concentrations. Analysis of dissolved organic carbon (DOC) was carried out at Umeå Marine
306 Science Center in Umeå, Sweden using a Shimadzu TOC-VcPH total organic carbon analyser.
307

The precipitates collected from the pump recovered from the HN-04 monitoring well were analysed by X-ray Powder Diffraction (XRD) at ISOR, Iceland for phase identification. The samples were measured using a Bruker AXS D8 Focus X-ray diffractometer with Cu kα radiation at 1.54Å wavelength, set at 40 kV and 40 mA using 1° divergence and receiving slits. The chemical composition of the precipitates was also analysed by ALS, Scandinavia. The precipitates were digested in HNO_3 and HCl with a trace of HF in a microwave oven. The resulting fluids were then analysed using both ICP-OES and High Resolution Inductively Coupled Plasma Mass Spectrometry (HR-ICP-MS). Detection limits were in the range of 0.01 ppm for trace elements to single ppm for major elements, and uncertainties for concentrations 10 times these detection limits are within 10% of the reported value.

Precipitates from samples collected from an air-lift of the HN-02 injection well in June 2013, were analysed for phase identification by XRD at the University of Copenhagen, Denmark with a Bruker D8 Discover equipped with a Co tube. 1L slurries collected from the air-lift were sealed immediately after sampling, transported to Denmark, where they were kept in an anaerobic chamber prior to analysis to minimise oxidation. Within the chamber, the samples were centrifuged, dried, crushed and mounted on low-background sample holders that were then covered with X-ray transparent cups to minimise oxidation during measurements.

Mass balance calculations

The fate of injected gases in this study are evaluated with the aid of mass balance calculations based on the injected non-reactive tracers SF_6 and SF_5CF_3 (Assayag et al., 2009; Matter et al., 2007; Matter et al., 2016). All collected water samples consist of a mixture from three sources; the original groundwater, that injected during Phase 1 and that injected during Phase 2. In the absence of reactions that remove or add material to the mixed fluid, mass balance requires that the concentration of chemical component *i* in the monitoring well samples (c_i) to be

$$c_i = c_{i,GW}X_{GW} + c_{i,1}X_{i,1} + c_{i,2}X_2 \qquad (1)$$

where $c_{i,GW}$, $c_{i,1}$, and $c_{i,2}$ refers to the concentration of the *i*th chemical component in the original groundwater, the Phase 1 injection and the Phase 2 injection, respectively, whereas and X_{GW}, X_1, and X_2 designate the fraction of the these three fluid sources in each monitoring sample.

The fraction of each water source in each monitoring sample was determined from the measured concentrations of the two non-reactive tracers, SF_6 and SF_5CF_3 together with the requirement that

$$X_{GW} + X_1 + X_2 = 1 \qquad (2)$$

Comparison of values based on the assumption of non-reactive mixing, obtained from Eqns. (1) and (2), with those measured in the monitoring wells provides an estimate of the percentage of injected gases fixed by chemical reactions, and the mass of elements added or removed from the fluid by mineral dissolution and precipitation reactions due to the injections. The background concentration of SF_6 in Eqn. 1 ($c_{i,GW}$) was not constant with time since SF_6 had been used in previous hydrological tests. This background concentration was corrected by taking account of the sample sodium fluorescein tracer concentrations; this tracer was co-injected with the SF_6 in the previous tests as described by Matter et al. (2016).

Sample 12KGM06 (Table 2) of the injected water from well HN-01 was used to constrain the elemental concentrations of the injected fluid, apart from the elements C and S, which were determined by accounting for the concentration of CO_2 and H_2S added to these injected fluids. Sample 12KGM01 (Table A1 in the electronic supplements) collected from well HN-04 before injection was used for representing the ambient groundwater concentrations. Mass balance calculations were performed for the major elements Ca, Mg, Si, Na, K, and Cl, and the trace elements Fe and Al.

Geochemical modelling

Modelling of the water chemistry, including the calculation of percent error in charge balance, the *in situ* saturation state of the water with respect to mineral and gas phases, and the effect of CO_2 and CO_2-H_2S-H_2 gas injection on the aqueous chemistry of the subsurface fluids

was performed using PHREEQC (Parkhurst and Appelo, 2013). In no case did the charge imbalance exceed 6.1%. The standard PHREEQC database was used in all calculations after including revised thermodynamic data on secondary minerals taken from Gysi and Stefánsson (2011), and pyrrotite and greigite taken from the MINTEQ and the llnl databases, respectively, as described in Alfredsson et al. (2013). Dissolved inorganic carbon (DIC) was calculated for each water sample using measured alkalinity, pH and temperature defined at 35°C at the *in situ* conditions. All saturation indices were calculated assuming the oxygen fugacity was controlled by equilibrium with the H_2S/SO_4^{2-} as a redox couple. For samples having no measured excess H_2S, the H_2S concentration was assumed to be equal to the detection limit of the H_2S titration, as geothermal waters always contain a small fraction of H_2S although below the detection limit.

Results

The compositions of all sampled fluids are shown in Figures 2, 3, and 8, Table 2 and Table A1 in the electronic supplements. An increase in the non-reactive sulphur hexafluoride (SF_6) tracer, indicating the initial arrival of the migrating dissolved CO_2 plume in the HN-04 monitoring well, occurred about two weeks after the start of the Phase I injection (Fig. 2a). The concentration of this tracer increased until a maximum 56 days after the Phase 1 injection started (Matter et al., 2016). The SF_6 tracer concentration again increased about 100 days after the injection started, reaching an overall maximum about 13 months after Phase I was started (see Fig 2a; Matter et al., 2016). This is the same pattern observed during the previous tracer test (Khalilabad et al., 2008), indicating that the storage formation consists of relatively homogenous porous media intersected by a low volume and fast flow path that channels about 3% of the tracer flow between wells HN-02 and HN-04. The same pattern was observed for Phase II, with the first arrival of the non-reactive trifluoromethyl sulphur pentafluoride (SF_5CF_3) tracer observed about two weeks after the start of the mixed-gas injection (Fig. 2a), with an initial smaller maximum about 60 days after the injection began (Matter et al., 2016). A further increase in SF_5CF_3 was noted about 150 days after Phase II injection began (Fig. 2a), consistent with the behaviour of SF_6 (Matter et al., 2016). The second SF_5CF_3 concentration maximum was not observed due to a breakdown of the submersible pump in the monitoring well HN-04, resulting in a three month gap in the monitoring data as described below.

Fluid pH, carbon, and sulphur

Prior to the injections, the pH of the HN-04 monitoring well samples was 9.5-9.6, the DIC was 1.3-1.4 mmol/L, and the total S concentration was 0.09-0.11 mmol/L (see Fig. 2b-c, Table A1 in the electronic supplements, and Alfredsson et al. (2013)). The measured pH and DIC before, during and after the two injection phases are shown in Figure 2b. The pH of the sampled fluids is extremely sensitive to the injection of dissolved gases. The pH *in situ* (35°C) decreases from 9.6 prior to each injection to approximately 7 near the end the injection then subsequently recovers to a value higher than 9. The decrease starts about two weeks after the start of Phase I, contemporary with the first arrival of the non-reactive tracer. The lowest pH following Phase I was 6.6 and occurred at the same time as the highest DIC value of 4.4 mmol/L, about 50 days after the Phase I injection was started, but ten days before the first reactive tracer maximum. Subsequently, both DIC and pH trended back towards their initial values (Fig. 2b). A similar pattern was observed during Phase II; the pH began to drop about two weeks after the injection was started, with the lowest pH of 7.1 measured at the same time as the highest DIC value of 3.3 mmol/L, about 60 days after the Phase II injection was started and concurrent the first SF_5CF_3 tracer maximum (see Fig 2).

No corresponding increase in DIC was observed during the second and larger SF_6 tracer maximum. This suggests significant mineral storage of the injected carbon; the difference between measured and calculated DIC indicate that >95% of the injected CO_2 was mineralised in less than two years, as previously reported by Matter et al. (2016). The second and larger SF_5CF_3 tracer maximum was not observed due to a pump failure in the HN-04 monitoring well, but an increase was noted in this concentration approximately one year after the start of the Phase II injection, consistent with the increase during the second breakthrough of SF_6. No corresponding increase in DIC was observed. Analysis of dissolved organic carbon (DOC) show continuous decrease in DOC concentrations from the start of Phase I, and throughout the monitoring period, except for a small increase shortly after the termination of the Phase II, from August to September 2012 (Table A1 in the electronic supplements). The measured DIC concentration is more than two orders of magnitude greater than the measured DOC concentration throughout most of the monitoring period after the Phase I injection (Fig. 2b and Table A1 in the electronic supplements).

The measured sulphur concentrations (SO_4^{-2}, H_2S, and S total) from before, during and after the Phase II injection are shown in Figure 2c and Table A1 in the electronic supplements. The concentrations are close to constant throughout this two year study. The average SO_4^{-2} concentration measured by IC-2000 during the period was 0.10±0.01 mmol/L, with a standard deviation of 0.005. The average total S concentration measured by ICP-OES was 0.10±0.02 mmol/L, with standard deviation of 0.003. The H_2S concentrations were, in most cases, close to the 0.3 µmol/L detection limit. The highest H_2S concentration, 1.5 µmol/L, was measured during the Phase II injection. The H_2S sulphur species always comprised less than 1.5% of the total dissolved S measured by the ICP-OES. This suggests an even more rapid mineralisation of the injected H_2S than the injected CO_2; no significant increase in sulphur concentrations was noted during this field injection experiment, indicating that all of the injected sulphur was mineralised before the first reactive tracer maximum of the SF_5CF_3 was observed in the monitoring well HN-04, or within 60 days of the start of the injection.

Major and trace elements

The release of the divalent cations Ca^{2+}, Mg^{2+}, and Fe^{2+} from the host basalt is essential for the mineralisation of the injected gases. The chemical compositions of the HN-04 monitoring samples demonstrate the rapid increase in Ca, Mg, and Fe concentration during the two injection phases with a gradual decline in the following weeks and months (see Fig. 3a-c). The increases in these concentrations were first observed concurrently with the first appearance of the non-reactive tracers. The Fe^{2+} was not detected in any sample after early April 2013, or about 6 weeks after the major part of the injected Phase 1 fluid arrived in well HN-04 and the Fe^{2+} concentrations were close to the detection limit for the two months following the start of the gas mixture injection.

In contrast, dissolved Si concentrations were close to constant throughout the monitoring period (Fig. 3d). An increase in Na concentration was most prominent at the beginning of the Phase I injection when its concentration increased from 2.1-2.2 mmol/L to about 2.3-2.4 mmol/L (Fig. 3e). Another increase was observed during the Phase II injection to about 2.5 mmol/L. The Na-concentration at the end of the monitoring period was about 2.6-2.7 mmol/L. A similar trend

461 is evident for K, but the increase in its concentration was somewhat lower than that of Na (Fig.
462 3f). The only major difference between the responses of these concentrations to the dissolved gas
463 injections was the presence of a small concentration peak in K during October 2012. The origin
464 of this peak in unclear. The Al concentrations were strongly pH dependent, consistent with its
465 solubility dependence on pH from neutral to basic conditions (e.g. Drever, 1982). As such, a
466 strong correlation was observed between Al concentrations and pH before, during, and after the
467 injections (Fig. 3g). The Cl concentrations were generally constant throughout the monitoring
468 period with a concentration of 2.4 mmol/L (Fig. h).
469

470 ## Calcite precipitates

471 In July 2013, about one and a half years after the start of the Phase I injection, the
472 submersible pump in well HN-04 broke down. When the pump was brought to the surface, it was
473 found to be clogged and coated with a green precipitate as shown in Figure 4. No precipitation
474 was observed on the pump prior to the injections. The bulk chemical compositions of the
475 precipitate samples are shown in Table 3. The cation concentration of the precipitates consisted
476 mostly of calcium (>94%) with some iron (<3%), silica (<2%) and magnesium (<1%). The
477 XRD-analysis (Fig. A2 in the electronic supplements) confirmed that calcite was the dominant
478 mineral phase of this precipitate and no other crystalline phases were identified. A ^{14}C analysis
479 of the carbon in the precipitates confirms that they originated from the injected ^{14}C labelled CO_2
480 (Matter et al., 2016).
481

482 ## Mineral saturation states of C- and S-bearing minerals

483 The saturation indices (SI) of calcite ($CaCO_3$), magnesite ($MgCO_3$) and siderite ($FeCO_3$),
484 as calculated using PHREEQC, are shown in Figure 5a. Calculations show that calcite was
485 saturated both before and after the Phase I and Phase II injections. This mineral was, however,
486 strongly undersaturated just after these injections concurrent with the drop in monitoring fluid
487 pH below 8, even though the DIC and Ca concentrations were relatively high (Figs. 2a and 3a).
488 Note that calcite was identified by XRD-analysis on drill-cuttings from the area prior to the
489 injections (Alfredsson et al., 2013) and within and on the pump in the monitoring well at the end
490 of the monitoring period (Figs. 4 and A2 in the electronic supplements). The monitoring fluid
491 samples attained calcite saturation at the end of April 2012, about seven weeks after the Phase I

injection was terminated, and at end of August, about four weeks after the Phase II injection was terminated, when the fluid pH had increased to >8. In contrast, the monitoring fluid samples were calculated to be supersaturated with respect to siderite shortly after both injections, whereas magnesite was strongly undersaturated during this time (Fig. 5a). Magnesite and siderite were not identified at the Hellisheidi site prior to the injections, but both minerals have been identified by XRD-analysis of drill-cuttings from the Svartsengi geothermal field in SW-Iceland (Franzson, 1983; Richter et al., 1999), which has a significantly higher salinity and higher temperature gradient than the CarbFix site. Magnesite-siderite solid solutions were identified in low temperature CO_2 metasomatised basalts in Nuussuaq, West Greenland (Rogers et al., 2006). There calcite appears at a relatively low CO_2 partial pressure, and magnesite-siderite at higher partial pressures (Fig. 6), as predicted by the PHREEQC modelling (Fig. 5a).

The calculated saturation indices of a number of other carbonate minerals are shown in Figure 5b. Ankerite ($CaFe(CO_3)_2$) is the only carbonate-phase that was supersaturated during the whole monitoring period, that is while Fe^{2+} concentrations are above the detection limit of the spectroscopic method. Ankerite has not been identified in the area. It was however identified during basaltic glass-CO_2 charged water interaction experiments performed at 75°C by Gysi and Stefánsson (2012b), and during basalt, water, supercritical CO_2 interaction experiments reported by McGrail et al. (2006). Similar to calcite, the sampled fluids were calculated to be supersaturated with respect to aragonite ($CaCO_3$) throughout the monitoring period, with the exception of several weeks near the end of, and shortly after both injections (see Fig. 5b). Aragonite was identified by XRD-analysis of drill-cuttings from the area prior to the injections (Alfredsson et al., 2013). Although the fluids were calculated to be supersaturated with respect to dolomite ($CaMg(CO_3)_2$) following both injections, this mineral has not been observed at the CarbFix site. It has been observed however by XRD-analysis as a secondary mineral in drill-cuttings from the saline Svartsengi high-temperature geothermal field in SW-Iceland, as is the case for magnesite and siderite (Franzson, 1983). The calculated saturation indices of three different Ca-Mg-Fe-solid solutions are shown in Figure 5c. All three show similar trends as calcite and aragonite. The $Mg_{0.50}$-$Fe_{0.50}$-CO_3 is the least saturated of the three, but attained saturation after both injections.

The calculated saturation indices for some sulphur-bearing minerals are shown in Figure 5d. The monitoring well fluids were calculated to be undersaturated with respect to native sulphur during the whole monitoring period. In contrast, pyrite (FeS_2), which is one of the most abundant secondary minerals at Hellisheidi at elevated temperature, and was identified at 780 m depth within the HN-02 injection well (Helgadóttir, 2011), was calculated to be supersaturated in all the monitoring fluid samples, showing a slight decrease in its saturation index at the beginning of the Phase II injection and a peak mid-August 2012 concurrent with the first maximum in SF_5CF_3 concentration, indicating the initial breakthrough of the injected Phase II fluids (Fig. 5d). As previously mentioned, calcite was the only crystalline phase identified in the precipitates forming on the pump from well HN-04. Pyrite was, however, identified by XRD-analysis on samples collected from an airlift of the injection well HN-02, confirming formation of pyrite during or after the Phase II injection (Fig. A3 in the electronic supplement). Greigite (Fe_3S4) showed a similar behaviour as pyrite, as this mineral was supersaturated in all monitoring well fluid samples. This mineral was not identified in the area previously, and was not identified by XRD analysis on the airlift samples collected from the injection well HN-02. It is, however, a metastable phase that may be a precursor of pyrite (Deer et al., 1992). Pyrrhotite (Fe_7S_8- FeS) was slightly supersaturated in the fluids sampled during the first weeks of the Phase II injection but undersaturated in all other samples (Fig. 5d). Pyrrhotite was previously identified within the high-temperature system in the Hellisheiði area (e.g. Gunnarsdóttir, 2012), but was not found at the CarbFix site nor identified in XRD analysis on the airlift samples from the injection well HN-02 (Fig. A3 in the electronic supplements). Gunnlaugsson and Arnórsson (1982) reported that below 180°C, geothermal waters in Iceland equilibrate with marcasite (FeS_2) instead of pyrite; marcasite is a pyrite dimorph generally found at lower temperatures (Deer et al., 1992). There was no evidence of marcasite in samples from the CarbFix site, either prior to the injections or in the XRD-analysis from the airlift pumping of well HN-02 (Fig. A3 in the electronic supplement). Mackinawite ($(Fe,Ni)_9S_8$) became supersaturated in the fluids sampled at the beginning of the Phase II injection, during the initial breakthrough of the injected Phase II fluid, and it is near to saturation in some monitoring samples collected from October to April 2013 (Fig. 5d). Mackinawite was not been identified in the area, and was not detected by XRD-analysis on the airlift samples from HN-02 (Fig. A3 in the electronic supplement).

However, mackinawite typically forms as a nanocrystalline material, whose broad peaks in XRD would be complicated to identify.

Saturation indices for other minerals

Saturation indices for other selected minerals are shown in Figure 7. Chalcedony (SiO_2) was slightly undersaturated in the monitoring fluid samples prior to the injections, but becomes saturated during Phase I; it then remains saturated for the rest of the monitoring period (Fig. 7a). Chalcedony is a common secondary mineral in the area (e.g. Alfredsson et al., 2013)

The mineral saturation states for those zeolites that are common in the area are shown in Figure 7b. Analcime, a common Na-zeolite found as an alteration phase at the CarbFix site, was undersaturated in the sampled fluids until about two months after the beginning of the Phase II injection, and then it is subsequently saturated (Fig. 7b). The samples were supersaturated with respect to other zeolites previously found in the area; and the general trend was a decrease in the monitoring fluid saturation index during the Phase I injection with an increase 6-8 weeks after Phase I was started. A slight dip was observed during the Phase II injection and an increase was observed during the second breakthrough of the injected fluid from Phase I (Fig. 7b).

The mineral saturation states for common clay minerals are shown in Figure 7c. Kaolinite ($Al_2Si_2O_5OH_4$) remained strongly supersaturated in the fluids sampled during the entire monitoring period (Fig. 7c), but increasingly so when the samples had a pH <8, during the injections and in the first weeks thereafter. Kaolinite was identified as a surface alteration product in geothermal areas (e.g. Markússon and Stefánsson, 2011) but has not been identified in subsurface samples collected from wells at Hellisheidi. The saturation state of gibbsite ($Al(OH)_3$) is depicted with the clay minerals; its behaviour was similar to kaolinite, except that it was undersaturated prior to the injections and became saturated when pH dropped below 8 during Phase I. It remained slightly supersaturated during the rest of the monitoring period (Fig. 7c). The saturation states of two other members of the kaolinite group; imogolite ($Al_2SiO_3OH_4$) and allophane ($Al_2O_3SiO_2*H_2O$), were also calculated. Imogolite was undersaturated prior to the injections but became strongly supersaturated during Phase I when the pH drops below 8, and remained supersaturated for the rest of the monitoring period, but decreasingly so as the pH

584 increased (Fig. 7c). Allophane was undersaturated during the whole monitoring period. Smectite
585 was supersaturated in all samples except for the samples taken during, and shortly after the two
586 injections while the pH was <8 (Fig. 7c). Smectite is one of the most abundant secondary
587 minerals in basaltic rocks and has been identified in all wells drilled at Hellisheidi (e.g.
588 Schiffman and Fridleifsson, 1991).
589
590 ## Discussion
591 Concentrations for the major elements Ca, Mg, Si, Na, K and Cl and the trace elements
592 Fe and Al calculated using equations (1) and (2), based on the assumption of non-reactive
593 conservative fluid mixing, are shown in Figure 3 together with their corresponding measured
594 concentrations. Corresponding plots for the injected constituents are shown in Figure 2.
595 Measured concentrations, greater than those calculated based on conservative fluid mixing,
596 suggest net dissolution, lower concentrations suggest net precipitation (i.e. “fixation”). Measured
597 Ca, Mg, and Fe concentrations were much higher during the injections and the subsequent days
598 and weeks than that calculated assuming non-reactive conservative mixing. This indicates a net-
599 input of these elements to the fluid consistent with the dissolution of the basalt originally present
600 in the reservoir. The measured concentrations of these elements eventually became lower, and in
601 the case of Mg, measured concentrations became lower than that calculated from non-reactive
602 mechanical mixing (Fig. 3b) about 300 days after the start of the Phase 1 injection, suggesting
603 net-precipitation into secondary minerals after these times.
604
605 Measured and calculated non-reactive conservative mixing concentrations of Si were
606 approximately identical during the first breakthrough of Phase I, but the measured concentrations
607 were lower during the second breakthrough (Fig. 3d). Measured Na and K concentrations were
608 higher than the calculated from non-reactive conservative mixing, with a continuous increase up
609 until the second breakthrough of Phase I, indicating net-release of these elements from the rock
610 to the fluid (Fig. 3e-f). Na and K are the most mobile major elements during the weathering and
611 low temperature alteration of basaltic rocks (Alfredsson et al., 2013; Eiriksdottir et al., 2015;
612 Gislason et al., 1996). Measured Al concentrations were much lower during Phase I than
613 corresponding calculated non-reactive conservative mixing concentrations indicating net Al
614 precipitation during the injection and during the following weeks, while the pH of the samples

from well HN-04 was below 8 (Fig. 3g). Subsequently, the measured Al concentration rises slowly, with a small drop during the Phase II injection. From about 300 days after the start of the Phase I injection, and throughout the sampling period, the measured Al concentration in the samples exceeded the corresponding calculated concentrations, indicating a net release of this element from the rocks. Chlorine is a trace element in basaltic rocks (Sigvaldason and Oskarsson, 1976), but is sparingly taken up by secondary minerals, providing an example of a mobile element that behaves conservatively during mechanical mixing and moderate water rock interactions (Arnórsson and Andrésdóttir, 1995; Gislason and Eugster, 1987; Olsson et al., 2014). Measured and calculated conservative mixing concentrations of Cl were approximately identical, except during the second breakthrough of Phase I, when the measured concentrations were slightly lower than the calculated values (Fig. 3h) suggesting its possible uptake into carbonates (Olsson et al., 2014).

The fate of the injected carbon

The results and calculations presented above provide insight into the fate of the injected dissolved CO_2 gas. As previously reported by Matter et al. (2016), the difference between the measured and calculated non-reactive mixing DIC concentration (Fig. 8a), indicates its loss along the flow-path towards the monitoring well. Matter et al. (2016) also suggest that the dissolution of pre-existing carbonates at the onset of the CO_2 injection may have contributed to the neutralisation of the injected CO_2-rich water, along with dissolution of other phases such as basaltic glass, primary minerals of the host rock and other secondary minerals. This liberation of cations and neutralization of the originally acidic gas-rich injected aqueous fluid lead to the precipitation of carbonate minerals; Matter et al. (2016) concluded that over 95% of the carbon injected during Phase I was fixed as carbonate minerals in less than two years.

These previous conclusions are supported by the observations reported in this study. Shortly after the injections, the measured concentrations of dissolved Mg, Fe, and Ca increased substantially (Fig. 3a-c), and were greatly above that computed for non-reactive mixing, consistent with the rapid dissolution of the original reservoir rock. The dissolved concentration of Ca in these fluids was far greater than that of Mg and Fe, suggesting the preferential dissolution of calcium bearing minerals, such as calcite, during and shortly after both injection

phases. Indeed, the saturation state of calcite, the major carbonate phase present in the basaltic reservoir became undersaturated during and just after the Phase I injection (Fig .5a), consistent with the initial dissolution of the calcite originally present in the host rock. Approximately 100 days after the start of the Phase I injection the monitoring fluid samples became supersaturated with respect to calcite with a saturation index of 0.6; this degree of supersaturation would be sufficient to grow calcite on the surfaces of the silicate minerals present in the reservoir (Stockmann et al., 2014). A similar variation of the calcite saturation state was evident following the Phase II injection. Moreover, calcite was observed to have precipitated within the monitoring well following the injection.

The saturation state of the monitoring fluid samples with respect to the carbonate phases magnesite and dolomite followed a similar pattern as calcite (Fig. 5b), but these were not identified in the study area. Such minerals have been reported to be kinetically inhibited from forming abiotically at temperatures less than 80 °C (Higgins and Hu, 2005; Kessels et al., 2000; Lippmann, 1973; Saldi et al., 2009, 2012). Similarly, siderite was calculated to be supersaturated in the sampled fluid but has not been found at the study site to date.

The fate of the injected sulphur

A noteworthy observation in this study is that the dissolved sulphur concentrations in the monitoring well samples remained close to constant during and after the injection of the H_2S-rich phase II injection. In contrast, non-reactive mixing calculations suggest these concentrations should have been as high as 0.6 mmol/L in the absence of sulphur precipitation (Fig. 8b). This indicates that vast majority of the sulphur injected into the subsurface was fixed within several weeks, before the Phase II fluids arrived at the first monitoring well. Indeed, numerous sulphur-bearing minerals, including pyrite, pyrrhotite, mackinawite, and greigite were supersaturated during the first weeks of Phase II injection (Fig. 5d).

Pyrite was strongly supersaturated favouring its nucleation and subsequent precipitation. The pyrite formation was confirmed by XRD-analysis on solids collected from the water samples taken during airlift from the injection well HN-02 in the spring of 2013. The analysis showed peaks from pyrite, amounting to 5-10 weight% of the solid material present in the air-lift

677 samples, based on Rietveld analysis using the software Topas (Fig. A3 in the electronic
678 supplement). No other well-crystalline sulphides were identified in these airlift samples.
679 Moreover, sulphide minerals were not identified in the precipitates recovered from the HN-04
680 monitoring well pump, which supports the conclusion that the H_2S mineralises prior to the
681 arrival of the injection fluid at the first monitoring well. This rapid mineralisation of the injected
682 H_2S is also in agreement with experimental studies on H_2S sequestration in basaltic rocks
683 (Gudbrandsson and Stefánsson, 2014).
684

685 ## The timescale of carbon and sulphur mineralisation: Carbon storage in
686 ## sedimentary basins versus basaltic rocks.

687 Carbon storage in sedimentary basins typically proceeds via the injection of pure CO_2
688 into porous sedimentary rocks (Fig. 9a). For common geothermal gradients, CO_2 is a
689 supercritical fluid below 800 m in sedimentary basins. As supercritical CO_2 is less dense than the
690 formation waters near this depth, it is buoyant and tends to rise to the surface. Ideally this CO_2 is
691 trapped below an impermeable cap rock via structural or stratigraphic trapping. Eventually some
692 of this CO_2 becomes stuck in small pores, limiting its mobility (residual trapping). Over time,
693 CO_2 dissolves in the formation water (solubility trapping). As CO_2 charged water is denser than
694 the original formation water, this CO_2-charged water will tend to sink. Some of this dissolved
695 CO_2 may react to form stable carbonate minerals (mineral trapping). As one progresses from
696 structural to mineral trapping, the CO_2 becomes more immobile and thus the storage more
697 secure, though this process can take thousands of years or more as summarized in Figure 9a
698 (Benson and Cole, 2008; Benson et al., 2005). Mineral trapping in sedimentary basins is slow
699 and sometimes limited because of a lack of the calcium, magnesium, and iron bearing minerals
700 required to mineralise the injected CO_2 (Gilfillan et al., 2009; Gislason and Oelkers, 2014).
701

702 In contrast during the CarbFix method, CO_2 is dissolved into water during its injection
703 into porous basaltic rocks. No cap rock is required because the dissolved CO_2 is not buoyant and
704 will not tend to migrate back to the surface. Solubility trapping occurs within 5 minutes during
705 the CO_2 injection process (Sigfusson et al., 2015), and due to the reactivity of the basaltic rocks
706 the bulk of the carbon is trapped in minerals within two years as shown in Figure 9b (this study;
707 Matter et al., 2016). This rapid carbonation of injected CO_2 provides a permanent and safe

carbon storage option; once fixed into a carbonate mineral, the risk of leakage is minimal and little if any further monitoring of the site will be necessary.

The results of this study suggest that the co-injection of H_2S with CO_2 into the subsurface both rapidly fixes this gas through pyrite precipitation and does not detrimentally effect the carbonation of the injected CO_2. Indeed, the results from this study indicate that this pyrite mineralization is even faster than the carbonate mineralization; the bulk of the sulphur is trapped in minerals within four months from injection. The co-injection of these two acid gases may provide a number of advantages, most notably, it may lower substantially the energy and cost required to capture and separate the CO_2 from industrial exhaust. This possibility is now being explored in the SulFix-CarbFix project , where a CO_2-H_2S gas mixture is being captured and separated from the gas stream of the Hellisheidi power plant by its dissolution in water at the surface at about 5 bars pressure and 20°C. The resulting gas charged water is directly injected to 700 m depth and 200 - 270°, aiming to store 8,000 - 10,000 tonnes of the gas mixture annually.

The degree to which the CarbFix method can be applied at other sites will depend on the availability of suitable host-rocks, sufficient water to dissolve the CO_2 during its injection, and economic considerations. This on-shore CarbFix project, demonstrates the feasibility of carbon storage in basaltic rocks. Nevertheless, the largest geological storage potential for CO_2 lies offshore (Goldberg and Slagle, 2009; Goldberg et al., 2010; Goldberg et al., 2008; Snæbjörnsdóttir et al., 2014), where the mid-oceanic ridges contain permeable basaltic layers and the oceans provide an unlimited reservoir for the required water (Snæbjörnsdóttir and Gislason, 2016).

Conclusions

This paper reported the chemical composition and mineral saturation states of fluids collected prior to, during and after the injection of 175 tonnes of pure CO_2 and 73 tonnes of a gas-mixture consisting of 75 mol% CO_2, 24 mol% H_2S and 1 mol% H_2, into basaltic rocks at the CarbFix site in SW-Iceland. All results indicate that the vast majority of injected CO_2 and H_2S were rapidly fixed within minerals in subsurface basalts. The results presented above confirm that this fixation occurred by the initial dissolution of the host basalts due to the injection of

acidic gas-charged water; mass balance indicates the net input from host rock dissolution of Mg, Fe, and Ca following each injection. The dissolution of host basalts and fluid mixing neutralized the pH of the injected fluid such that calcite became supersaturated approximately 100 days after the start of each injection favouring the fixation of the injected CO_2 within this mineral. This results, which supports those of Matter et al. (2016) who concluded that CO_2 mineralization fixed over 95% of the injected carbon within 2 years, was further validated by observations of calcite precipitation within the monitoring well itself. Although other metal carbonate minerals, notably, ankerite, siderite and mixed Ca, Mg, Fe-carbonates, were also supersatutated in the monitoring fluids these were not observed to form during this study.

Similar results support the even more rapid mineralization of injected H_2S as pyrite, as this mineral is supersaturated before, during and after the injection of a mixed CO_2-H_2S charged water into the basalts. The rapid fixation of H_2S into this mineral is further evidenced by the observation of pyrite precipitation in the injection well but not in the first monitoring well. Such observations suggest that H_2S fixation by pyrite precipitation was essentially complete before the injected mixed-gas plume arrived at the monitoring well. Notably there appears to have been little difference in the chemical response in the subsurface of the mixed H_2S-CO_2 gas mixture injection compared to that of the pure CO_2 injection. Their similar success towards the CO_2 mineralization suggests that the injection of mixed gases might prove to be a simpler and more cost-effective approach to subsurface carbon storage than the injection of pure CO_2.

Acknowledgement

We acknowledge funding from the Reykjavik Energy; Environmental Fund of Reykjavik Energy; the European Commission through the projects CarbFix (EC coordinated action 283148), Min-GRO (MC-RTN-35488), Delta-Min (PITN-GA-2008-215360), and CO_2-REACT (EC Project 317235); the U.S. Department of Energy under award number DE-FE0004847; Nordic fund 11029-NORDICCS; and the Icelandic GEORG Geothermal Research fund (09-02-001). We are indebted to Hólmfríður Sigurðardóttir and Bergur Sigfússon at Reykjavík Energy, Magnús Þór Arnarson at Mannvit Engineering, Domenik Wolff-Boenisch at Curtin University in Australia, Helgi A. Alfreðsson at the University of Iceland and Wallace S. Broecker at Columbia University for their contributions to the CarbFix project. We thank Einar Örn Þrastarson, Trausti

Kristinsson, Vordís Eiríksdóttir, Halldór Bergmann, and Þorsteinn A. Þorgeirsson at Reykjavík Energy; Vigdís Harðardóttir, Finnbogi Óskarsson, Kristján Hrafn Sigurðsson and Steinþór Níelsson at ISOR; Jennifer Hall at Columbia University, and Þorsteinn Jónsson, Sveinbjörn Steinþórsson, Iwona Galezcka, Eydís S. Eiríksdóttir, Deirdre Clark, Chris Grimm and Flora Brocza at the University of Iceland for helping the injection and sampling campaign. We also are grateful for the assistance of Rósa Ólafsdóttir at the University of Iceland. Finally, the first author would like to thank Becca Neely for all her help and assistance in the field, in the lab and in our office.

References

Alfredsson, H. A., Oelkers, E. H., Hardarsson, B. S., Franzson, H., Gunnlaugsson, E., and Gislason, S. R., 2013. The geology and water chemistry of the Hellisheidi, SW-Iceland carbon storage site: International Journal of Greenhouse Gas Control, v. 12, p. 399-418.

Aradóttir, E. S. P., Gunnarsson, I., Sigfússon, B., Gislason, S. R., Oelkers, E. H., Stute, M., Matter, J. M., Snæbjörnsdóttir, S. Ó., Mesfin, K. G., Alfredsson, H. A., Hall, J., Arnarsson, M. T., Dideriksen, K., Júlíusson, B. M., Broecker, W. S., and Gunnlaugsson, E., 2015. Towards Cleaner Geothermal Energy: Subsurface Sequestration of Sour Gas Emissions from Geothermal Power Plants, Proceedings World Geothermal Congress 2015: Melbourne, Australia, 19-25 April 2015.

Aradóttir, E. S. P., Sonnenthal, E. L., Björnsson, G., and Jónsson, H., 2012. Multidimensional reactive transport modeling of CO_2 mineral sequestration in basalts at the Hellisheidi geothermal field, Iceland: International Journal of Greenhouse Gas Control, v. 9, p. 24-40.

Archer, D., 2005. Fate of fossil fuel CO_2 in geologic time: Journal of Geophysical Research, v. 110, p. C09S05.

Arnórsson, S., and Andrésdóttir, A., 1995. Processes controlling the distribution of boron and chlorine in natural waters in Iceland: Geochimica et Cosmochimica Acta, v. 59, no. 20, p. 4125-4146.

Arnórsson, S., D'Amore, F., and Gerardo-Abaya, J., 2000. Isotopic and geochemical techniques in geothermal exploration, development and use: Sampling methods, data handling, interpretation. Arnórsson, S. (Ed.), International Atomic Energy Agency Publication, Vienna.

Assayag, N., Matter, J., Ader, M., Goldberg, D., and Agrinier, P., 2009. Water–rock interactions during a CO_2 injection field-test: Implications on host rock dissolution and alteration effects: Chemical Geology, v. 265, no. 1–2, p. 227-235.

Bachu, S., and Gunter, W. D., 2005. Overview of acid-gas injection operations in Western Canada, *in* Wilson, E. S., Rubin, D. W., Keith, C. F., Gilboy, M., Thambimuthu, T., Morris, J., and Gale, K., eds., Greenhouse Gas Control Technologies 7: Oxford, Elsevier Science Ltd, p. 443-448.

Bacon, D. H., Ramanathan, R., Schaef, H. T., and McGrail, B. P., 2014. Simulating geologic co-sequestration of carbon dioxide and hydrogen sulfide in a basalt formation: International Journal of Greenhouse Gas Control, v. 21, p. 165-176.

Benson, S.M. and Cook, P., Coordinating Lead Authors. Anderson, J., Bachu,S., Nimir, H.B., Basu, B., Bradshaw, J., Deguchi, G., Gale, J., von Goerne, G., Heidug, W., Holloway, S., Kamal, R., Keith, D., Lloyd, P., Rocha, P., Senior, B., Thomson, J., Torp, T., Wildenborg, T., Wilson, M., Zarlenga, F., and Zhou, D, Lead Authors. Celia, S.M., Gunter, B., Ennis King, J., Lindegerg, E., Lombardi, S., Oldenburg, C., Pruess, K., Rigg, A., Stevens, S., Wilson, E., Whittaker, S., 2005. Underground Geological Storage, IPCC Special Report on Carbon Dioxide Capture and Storage, Chapter 5. Intergovernmental Panel on Climate Change, Cambridge University Press, Cambridge, U.K.

Benson, S. M., and Cole, D. R., 2008. CO_2 Sequestration in Deep Sedimentary Formations: Elements, v. 4, p. 325-331

Broecker, W., 2007. Climate change: CO_2 arithmetic: Science, v. 315, p. 1371.

Broecker, W. S., and Kunzig, R., 2008. Fixing climate. The story of climate science—and how to stop global warming. Green Profile.

Deer, W. A., Howie, R. A., and Zussman, J., 1992. An introduction to the rock forming minerals. 2nd edition, Harlow, England, Pearson, Prestice Hall, 696 p.

Drever, J. I., 1982. The Geochemistry of Natural Waters, Englewood Cliffs, N. J., Prentice-Hall.

Eiriksdottir, E. S., Gislason, S. R., and Oelkers, E. H., 2015. Direct evidence of the feedback between climate and nutrient, major, and trace element transport to the oceans: Geochimica et Cosmochimica Acta, v. 166, p. 249-266.

European Environment Agency, 2014. Sulphur dioxide (SO_2) emissions (APE 001) - Assessment published in Jan 2014. Volume 2015, European Environment Agency.

828 Fisher, A. T., 1998. Permeability within basaltic oceanic crust: Reviews of Geophysics, v. 36, no. 2, p.
829 143-182.
830 Flaathen, T. K., Gislason, S. R., Oelkers, E. H., and Sveinbjörnsdóttir, Á. E., 2009. Chemical evolution of
831 the Mt. Hekla, Iceland, groundwaters: A natural analogue for CO_2 sequestration in basaltic rocks:
832 Applied Geochemistry, v. 24, no. 3, p. 463-474.
833 Franzson, H., 1983. Svartsengi, well SG-12: Drilling, stratigraphy and aquifers (in Icelandic): National
834 Energy Authority of Iceland, OS/83003/JHD-02.
835 Galeczka, I., Wolff-Boenisch, D., Oelkers, E. H., and Gislason, S. R., 2014. An experimental study of
836 basaltic glass–H_2O–CO_2 interaction at 22 and 50°C: Implications for subsurface storage of CO_2:
837 Geochimica et Cosmochimica Acta, v. 126, p. 123-145.
838 Gensemer, R. W., and Playle, C., 1999, The bioavailability and toxicity of aluminum in aquatic
839 environments: Critical Reviews in Environmental Science and Technology, v. 29, no. 4, p. 315-
840 450.
841 Gilfillan, S. M. V., Lollar, B. S., Holland, G., Blagburn, D., Stevens, S., Schoell, M., Cassidy, M., Ding,
842 Z., Zhou, Z., Lacrampe-Couloume, G., and Ballentine, C. J., 2009. Solubility trapping in
843 formation water as dominant CO_2 sink in natural gas fields: Nature, v. 458, no. 7238, p. 614-618.
844 Gislason, S. R., Arnórsson, S., and Ármannsson, H., 1996. Chemical weathering of basalt in SW Iceland:
845 Effects of runoff, age of rocks and vegetative/glacial cover: American Journal of Science, v. 296,
846 p. 837-907.
847 Gislason, S. R., Broecker, W. S., Gunnlaugsson, E., Snæbjörnsdóttir, S. Ó., Mesfin, K. G., Alfredsson, H.
848 A., Aradottir, E. S., Sigfusson, B., Gunnarsson, I., Stute, M., Matter, J. M., Arnarson, M. T.,
849 Galeczka, I. M., Guðbrandsson, S., Stockman, G., Wolff-Boenisch, D., Stefansson, A.,
850 Ragnheidardottir, E., Faathen, T., Gysi, A. P., Olssen, J., Didriksen, K., Stippe, S., Menez, B.,
851 and Oelkers, E. H., 2014. Rapid solubility and mineral storage of CO_2 in basalt: Energy Procedia,
852 v. 63, p. 4561-4574.
853 Gislason, S. R., and Eugster, H. P., 1987. Meteoric water-basalt interactions. I: A laboratory study:
854 Geochimica et Cosmochimica Acta, v. 51, no. 10, p. 2827-2840.
855 Gislason, S. R., and Oelkers, E. H., 2014. Carbon Storage in Basalt: Science, v. 344, p. 373-374.
856 Gislason, S. R., and Torssander, P., 2006. Response of Sulfate Concentration and Isotope Composition in
857 Icelandic Rivers to the Decline in Global Atmospheric SO_2 emissions into the North Atlantic
858 Region: Environmental Science and Technology, v. 40, p. 680-686.
859 Gislason, S. R., Wolff-Boenisch, D., Stefansson, A., Oelkers, E. H., Gunnlaugsson, E., Sigurdardottir, H.,
860 Sigfusson, B., Broecker, W. S., Matter, J., Stute, M., Axelsson, G., and Fridriksson, T., 2010.
861 Mineral sequestration of carbon dioxide in basalt: A preinjection overview of the CarbFix project:
862 International Journal of Greenhouse Gas Control, v. 4, p. 537-545.
863 Global CCS Institute, 2015. The global Status of CCS 2015 – summary report. Melbourne, Australia.
864 Goldberg, D., Lackner, K., Han, P., and Wang, T., 2013, Co-Location of Air Capture, Subseafloor CO_2
865 Sequestration, and Energy Production on the Kerguelen Plateau: Environmental Science and
866 Technology, v. 47, no. 13.
867 Goldberg, D., and Slagle, A. L., 2009. A global assessment of deep-sea basalt sites for carbon
868 sequestration: Energy Procedia, v. 1, p. 3675-3682.
869 Goldberg, D. S., Kent, D. V., and Olsen, P. E., 2010. Potential on-shore and off-shore reservoirs for CO_2
870 sequestration in Central Atlantic magmatic province basalts: Proceedings of the National
871 Academy of Sciences of the United States of America Sciences, v. 107, p. 1327-1332.
872 Goldberg, D. S., Takahashi, T., and Slagle, A. L., 2008. Carbon dioxdie sequestration in deep-sea basalt:
873 PNAS, v. 105, no. 29, p. 9920-9925.
874 Gudbrandsson, S., and Stefánsson, A., 2014. Experimental study of H_2S sequestration in geothermal
875 systems, RH-14-2014.
876 Gudbrandsson, S., Wolff-Boenisch, D., Gislason, S. R., and Oelkers, E. H., 2011. An experimental study
877 of crystalline basalt dissolution from $2 < pH < 11$ and temperatures from 5 to 75 °C: Geochimica
878 et Cosmochimica Acta, v. 75, no. 19, p. 5496-5509.

Gunnarsdóttir, S. H., 2012. The Geology and Hydrothermal Alteration near the Mt. Reykjafell area in the Hellisheidi Geothermal Field. (MSc thesis). University of Iceland.
Gunnarsson, I., Sigfusson, B., Stefansson, A., Arnorsson, S., Scott, S., and Gunnlaugsson, E., 2011. Injection of H_2S from Hellisheiði Power Plant, Iceland, Workshop on Geothermal Reservoir Engineering: Stanford, California.
Gunnlaugsson, E., and Arnòrsson, S., 1982. The chemistry of iron in geothermal systems in iceland: Journal of Volcanology and Geothermal Research, v. 14, no. 3–4, p. 281-299.
Gysi, A. P., and Stefánsson, A., 2011. CO_2–water–basalt interaction. Numerical simulation of low temperature CO_2 sequestration into basalts: Geochimica et Cosmochimica Acta, v. 75, no. 17, p. 4728-4751.
-, 2012a. CO_2-water–basalt interaction. Low temperature experiments and implications for CO_2 sequestration into basalts: Geochimica et Cosmochimica Acta, v. 81, p. 129-152.
-, 2012b. Mineralogical aspects of CO_2 sequestration during hydrothermal basalt alteration — An experimental study at 75 to 250°C and elevated pCO_2: Chemical Geology, v. 306–307, p. 146-159.
Harris, R. N., and Chapman, D. S., 2004. Deep-seated oceanic heat flux, heat deficits and hydrothermal circulation, Cambridge, Cambridge University Press, Hydrogeology of the Oceanic Lithosphere.
Helgadóttir, H. M., 2011, Stratigraphy and hydrothermal alteration of the Gráuhnúkar geothermal system in the southern part of the Hengill area. (MSc Thesis). University of Iceland, 123 p.
Higgins, S. R., and Hu, X., 2005. Self-limiting growth on dolomite: Experimental observations with *in situ* atomic force microscopy: Geochimica et Cosmochimica Acta, v. 69, p. 2085-2094.
Hjartarson, Á., and Sæmundsson, K., 2014. Geological Map of Iceland. Bedrock. 1:600 000: Iceland GeoSurvey.
Hoffert, M., Caldeira, K., Benford, G., Criswell, D., Green, C., Herzog, H., Jain, A., Kheshgi, H., Lackner, K., Lewis, J., Lightfood, H., Manheimer, W., Mankins, J., Mauel, M., Perkins, L., Schlesinger, M., Volk, T., and Wigley, T., 2002, Advanced technology paths to global climate stability: energy for a greenhouse planet.: Science, v. 298, no. 981-987.
International Engy Agency, 2015. Mobilising Innovation to Accelerate Climate Action, Executive Summary.
IPCC, 2005. IPCC Special Report on Carbon Dioxide Capture and Storage. Prepared by Working Group III of the Intergovernmental Panel on Climate Change . Metz, B., Davidson, O., de Coninck, H.C., Loos, M., and Meyer, L. A. (eds.). Cambridge University Press, Cambridge, United Kingdom and New York, NY, USA, 442 pp.
-, 2014. Contribution of Working Groups I, II and III to the Fifth Assessment Report of the Intergovernmental Panel on Climate Change.
Kessels, L. A., Sibley, D. F., and Nordeng, S. H., 2000. Nanotopography of synthetic and natural dolomite crystals.: Sedimentology, v. 47, p. 173-186.
Khalilabad, M. R., Axelsson, G., and Gislason, S. R., 2008. Aquifer characterization with tracer test technique; permanent CO_2 sequestration into basalt, SW Iceland: Mineralogical Magazine, v. 72, p. 121-125.
Knauss, K.G., Johnson, J.W., Steefel, C.I., 2005. Evaluation of the impact of CO_2, co-contaminant gas, aqueous fluid and reservoir rock interactions on the geologic sequestration of CO_2. Chemical Geology, v. 217, no. 3–4, p. 339–350.
Lackner, K., 2003. A guide to CO_2 sequestration.: Science v. 300, p. 1677–1678.
Lippmann, F., 1973. Sedimentary carbonate minerals., New York, Springer-Verlag.
Markússon, S. H., and Stefánsson, A., 2011. Geothermal surface alteration of basalts, Krýsuvík Iceland—Alteration mineralogy, water chemistry and the effects of acid supply on the alteration process: Journal of Volcanology and Geothermal Research, v. 206, no. 1–2, p. 46-59.
Matter, J., Takahashi, T., and Goldberg, D., 2007. Experimental evaluation of *in situ* CO_2-water-rock reactions during CO_2 injection in basaltic rocks: Implications for geological CO_2 sequestration: Geochem Geophy Geosy 6, v. 8, no. 2, p. 19.

Matter, J. M., Broecker, W., Gislason, S. R., Gunnlaugsson, E., Oelkers, E., Stute, M., Sigurdardóttir, H., Stefansson, A., Wolff-Boenisch, D., Axelsson, G., and Sigfússon, B., 2011. The CarbFix Pilot Project - Storing Carbon Dioxide in Basalt: Energy Procedia v. 4, p. 5579-5585.

Matter, J. M., Stute, M., Snæbjörnsdóttir, S. Ó., Oelkers, E. H., Gislason, S. R., Aradottir, E. S., Sigfusson, B., Gunnarsson, I., Sigurdardottir, H., Gunnlaugsson, E., Axelsson, G., Alfredsson, H. A., Wolff-Boenisch, D., Mesfin, K., Fernandez de la Reguera Taya, D., Hall, J., Dideriksen, K., and Broecker, W. S., 2016. Rapid carbon mineralisation for permanent and safe disposal of anthropogenic carbon dioxide emissions: Science. Accepted.

McGrail, B. P., Freeman, C. J., Brown, C. F., Sullivan, E. C., White, S. K., Reddy, S., Garber, R. D., Tobin, D., Gilmartin, J. J., and Steffensen, E. J., 2012. Overcoming business model uncertainty in a carbon dioxide capture and sequestration project: Case study at the Boise White Paper Mill: International Journal of Greenhouse Gas Control, v. 9, p. 91-102.

McGrail, B. P., Schaef, H. T., Ho, A. M., Chien, Y.-J., Dooley, J. J., and Davidson, C. L., 2006. Potential for carbon dioxide sequestration in flood basalts: Journal of Geophysical Research v. Solid Earth (111), no. B12201.

McGrail, B. P., Spane, F. A., Sullivan, E. C., Bacon, D. H., and Hund, G., 2011. The Wallula basalt sequestration pilot project: Energy Procedia, v. 4, p. 5653-5660.

Oelkers, E., and Schott, J., 2005. Geochemical aspects of CO_2 sequestration.: Chemical Geology, v. 217, p. 183–186.

Oelkers, E. H., and Cole, D. R., 2008. Carbon dioxide sequestration: a solution to a global problem.: Elements, v. 4, p. 305–310.

Oelkers, E. H., Gislason, S. R., and Matter, J., 2008. Mineral carbonation of CO_2.: Elements, v. 4, p. 331–335.

Olsson, J., Stipp, S. L. S., Makovicky, E., and Gislason, S. R., 2014. Metal scavenging by calcium carbonate at the Eyjafjallajökull volcano: A carbon capture and storage analogue: Chemical Geology, v. 384, p. 135-148.

Pacala, S., and Socolow, R., 2004. Stabilization wedges: solving the climate problem for the next 50 years with current technologies: Science, v. 305, no. 968-971.

Parkhurst, D. L., and Appelo, C. A. J., 2013. Description of input and examples for PHREEQC version 3—A computer program for speciation, batch-reaction, one-dimensional transport, and inverse geochemical calculations, U.S. Geological Survey Techniques and Methods, v. chap. A43, 497 p.

Richter, B., Guðlaugsson, S. Þ., Steingrímsson, B., Björnsson, G., Bjarnason, J. Ö., and Þórhallson, S., 1999. Svartsengi well SJ-18: Drilling, research and production (in Icelandic), OS-99117.

Rogers, K. L., Neuhoff, P. S., Pedersen, A. K., and Bird, D. K., 2006. CO_2 metasomatism in a basalt-hosted petroleum reservoir, Nuussuaq, West Greenland: Lithos, v. 92, no. 1–2, p. 55-82.

Rosenbauer, R. J., Thomas, B., Bischoff, J. L., and Palandri, J., 2012. Carbon sequestration via reaction with basaltic rocks: Geochemical modelling and experimental results: Geochimica et Cosmochimica Acta, v. 89, p. 116−133.

Rutqvist, J., Birkholzer, J., Cappa, F., and Tsang, C.-F., 2007. Estimating maximum sustainable injection pressure during geological sequestration of CO_2 using coupled fluid flow and geomechanical fault-slip analysis. : Energy Conversion and Management, v. 48, p. 1798–1807.

Saldi, D., Jordan, G., Schott, J., and Oelkers, E. H., 2009. Magnesite growth rates as a function of temperature and saturation state.: Geochim. Cosmochim. Acta v. 73, p. 5646–5657.

Saldi, G. D., Schott, J., Pokrovsky, O. S., Gautier, Q., and Oelkers, E. H., 2012. An experimental study of magnesite precipitation rates at neutral to alkaline conditions and 100–200 C as a function of pH, aqueous solution composition and chemical affinity: Geochimica et Cosmochimica Acta, v. 83, p. 93-109.

Schiffman, P., and Fridleifsson, G. O., 1991. The smectite-chlorite transition in drillhole NJ-15, Nesjavellir Geothermal Field, Iceland: XRD, BSE and electron microprobe investigations: Journal of Metamorphic Geology, v. 9, no. 6, p. 679-696.

Sigfusson, B., Gislason, S. R., Matter, J. M., Stute, M., Gunnlaugsson, E., Gunnarsson, I., Aradottir, E. S., Sigurdardottir, H., Mesfin, K. G., Alfredsson, H. A., Wolff-Boenisch, D., Arnarson, M. T., and Oelkers, E. H., 2015. Solving the carbon-dioxide buoyancy challenge: The design and field testing of a dissolved CO_2 injection system: Int. J. Greenhouse Gas Control, v. 37, p. 213-219.

Sigvaldason, G. E., and Oskarsson, N., 1976. Chlorine in basalts from Iceland: Geochim. Cosmochim. Acta, v. 40, p. 777-789.

Smith, S. J., Van Aardenne, J., Klimont, Z., Anders, R. J., Volke, A., and Delgato Arias, S., 2011. Anthropogenic sulfur dioxide emissions 1850-2005: Amospheric Chemistry and Physics, v. 11, p. 1101-1116.

Snæbjörnsdóttir, S. Ó., and Gislason, S. R., 2016. CO_2 storage potential of basaltic rocks offshore Iceland: Energy Procedia, v. 86, p. 371-380.

Snæbjörnsdóttir, S. Ó., Wiese, F., Fridriksson, T., Ármannsson, H., Einarsson, G. M., and Gislason, S. R., 2014. CO_2 storage potential of basaltic rocks in Iceland and the oceanic ridges: Energy Procedia, v. 63, p. 4585-4600.

Stefánsson, A., Arnórsson, S., Gunnarsson, I., Kaasalainen, H., and Gunnlaugsson, E., 2011. The geochemistry and sequestration of H_2S into the geothermal system at Hellisheidi, Iceland: Journal of Volcanology and Geothermal Research, v. 202, no. 3–4, p. 179-188.

Stockmann, G. J., Wolff-Boenisch, D., Bovet, N., Gislason, S. R., and Oelkers, E. H., 2014. The role of silicate surfaces on calcite precipitation kinetics: Geochimica et Cosmochimica Acta, v. 135, p. 231-250.

Stockmann, G. J., Wolff-Boenisch, D., Gislason, S. R., and Oelkers, E. H., 2011. Do carbonate precipitates affect dissolution kinetics? 1: Basaltic glass: Chemical Geology, v. 284, no. 3–4, p. 306-316.

Stockmann, G. J., Wolff-Boenisch, D., Gislason, S. R., and Oelkers, E. H., 2013. Do carbonate precipitates affect dissolution kinetics?: 2: Diopside: Chemical Geology, v. 337–338, p. 56-66.

Stumm, W., and Morgan, J. J., 1996. Aquatic Chemistry: Chemical equilibria and rates in natural waters (third ed.), John Wiley & Sons, New York, 1022 p.:

Thorarinsson, S. B., Helgadóttir, H. M., Franzson, H., Harðarson, B. S., Hjartarson, A., Ásmundsson, R., and Sigurdsson, G., 2006. Hellisheidi - well HN-04. 1st to 3rd stages: Drilling of 18 5/8" security casing in 105 m, production casing in 400 m and 12 1/4" production part in 1204 m: ISOR, Iceland GeoSurvey, ISOR-2006/055.

United States Environmental Protection Agency, 2015. The National Emissions Inventory. National Summary of Sulfur Dioxide Emissions, NEI 2011 v2 GPR.

Van Pham, H., Aagaard, P., and Hellevang, H., 2012. On the potential for CO_2 mineral storage in continental flood basalts - PHREEQC batch and 1D diffusion - reaction simulations: Geochemical Transactions, v. 13, no. 5, p. 12.

Wiese, F., Fridriksson, T., and Armannsson, H., 2008. CO_2 Fixation by Calcite in High-temperature Geothermal Systems in Iceland: ISOR, Iceland Geosurvey, ISOR−2008/003

Wolff-Boenisch, D., Wenau, S., Gislason, S. R., and Oelkers, E. H., 2011. Dissolution of basalts and peridotite in seawater, in the presence of ligands, and CO_2: Implications for mineral sequestration of carbon dioxide: Geochimica et Cosmochimica Acta, v. 75, no. 19, p. 5510-5525.

World Health Organization, 2000. WHO air quality guidelines for Europe, 2nd edition: WHO regional office for Europe.

WorleyParsons, and Schlumberger, 2011. Assessment of Carbon Capture and Storage Technologies: 2011, update: Global CCS Institute.

Wöll, C., Hallsdóttir, B. S., Guðmundsson, J., Snorrason, A., Þórsson, J., Jónsson, P. V. K., Andrésson, K., and Einarsson, S., 2014. Emissions of greenhouse gases in Iceland from 1990 to 2012. National Inventory report 2014.: Environment Agency of Iceland, UST-2014-2.

Tables

Table 1. Characteristics of the two gas injections into the CarbFix storage site considered in this study.

	Phase I: Injection of 100% CO_2	**Phase II: Injection of 75% CO_2, 24% H_2S, 1% H_2**
Period:	24th of January to 9th March 2012	15th of June to 1st of August 2012
Injection period (days)	45 Active: 40	48 Active: 29
Mass of injected gas (Tonnes)	175	73
Tracers:		
Reactive	^{14}C	^{14}C
Concentration:	40.0 Bq/L*	6 Bq/L*
^{14}C:^{12}C ratio	2.16 x 10^{-11}*	6.5 x 10^{-12}*
Non-reactive	SF_6	SF_5CF_3
Concentration:	2.33 x 10^{-8} ccSTP/cc*	2.24 x 10^{-8} ccSTP/cc*

**From Matter et al. 2016*

Table 2. The measured chemical composition of water collected from well HN-01, and co-injected with pure CO_2 gas or CO_2/H_2S gas mixtures into the CarbFix storage site.

Date	Sample ID	pH	Conductivity	H_2S	O_2	Alk.	DIC	$S_{(total)}$
			µs/cm	*µmol/L*	*mmol/L*	*mmol/L*	*mmol/L*	*mmol/L*
3.2.2012	12KGM06	9.29	292	0.45	0.051	2.109	1.460	0.118
4.7.2012	12SOS03	9.21	300	0.32*	0.082	2.046	1.550	0.085

Date	Sample ID	pH	Ca	Mg	Fe	Si	Na	K	Al	Cl
			mmol/L	*mmol/L*	*µmol/L*	*mmol/L*	*mmol/L*	*mmol/L*	*µmol/L*	*mmol/L*
3.2.2012	12KGM06	9.29	0.13	0.16	0.021	0.59	2.04	0.024	1.19	0.31
4.7.2012	12SOS03	9.21	0.15	0.20	0.068	0.39	1.83	0.024	0.65	0.25

*Measured on 12th of July

Table 3. The measured chemical composition of the major elements of two solid samples collected from the water pump recovered from well HN-04 on the 13th of August 2013.

Si mmol/L	**Na** mmol/L	**K** mmol/L	**Ca** mmol/L	**Mg** mmol/L	**S** mmol/L	**Al** mmol/L	**Fe** mmol/L
185	14.8	1.00	9482	136	10.0	0.03	286.5
171	11.3	0.49	10230	123	5.3	0.02	197.0

Figures

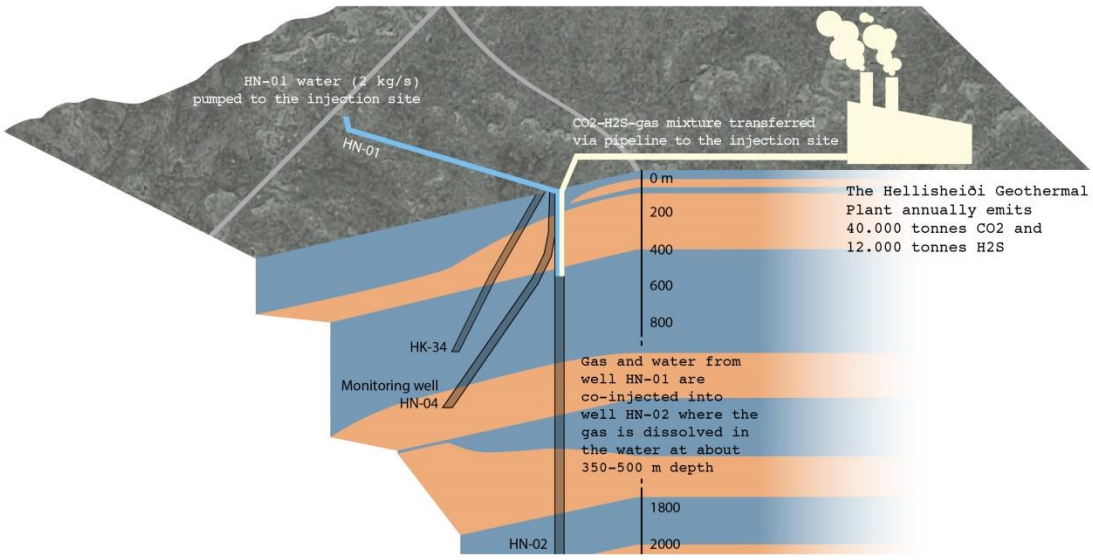

Figure 1. Geological cross section of the CarbFix injection site, modified from Alfredsson et al. (2013). Blue indicates lava flows and brown indicates hyaloclastic (glassy) formations. The CO_2-H_2S-H_2 gas mixture used in the second injection was separated from other geothermal gases at the power plant and transported via gas pipe to the injection site where it was dissolved in water from well HN-01 within the injection well HN-02. The gas charged water enters the basalts as a single phase. Water was pumped from well HN-01 to the injection well HN-02 at the rate of 7.2 m^3/h. Water was pumped from the monitoring well at the rate of 3.5 m^3/h, throughout this study. Graphic work by Sölvi Snæbjörnsson.

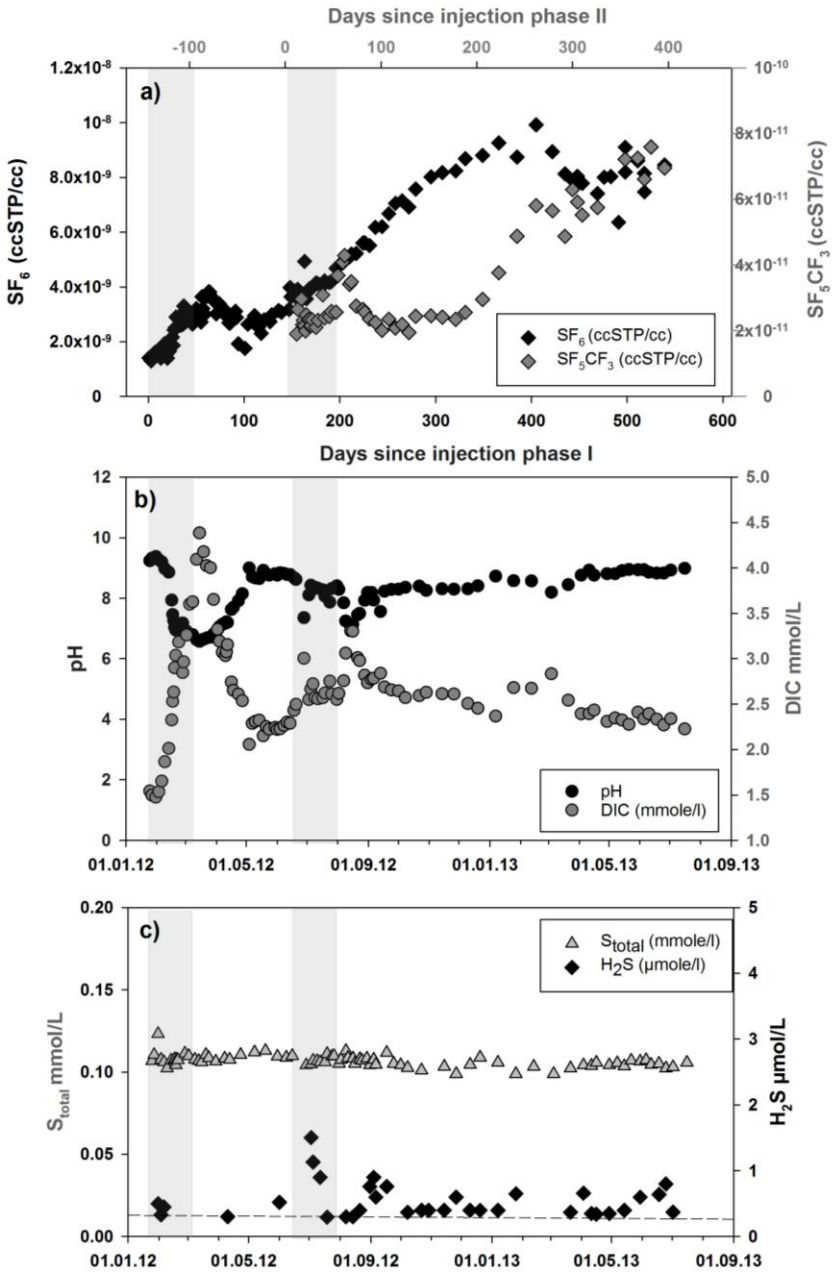

Figure 2. Concentrations of a) SF_6 and SF_5CF_3 non-reactive tracers; b) dissolved inorganic carbon (DIC) along with fluid pH calculated at *in situ* temperature (35°C), c) total dissolved sulphur and $H_2S_{(aq)}$ in samples from monitoring well HN-04 prior to, during, and after the injection of pure CO_2 and mixed CO_2/H_2S gas into the CarbFix Storage site. The timing of both gas injections is indicated by grey bars. The detection limit of the H_2S concentration measurements is 0.3 µmol/L and is indicated as a dotted line.

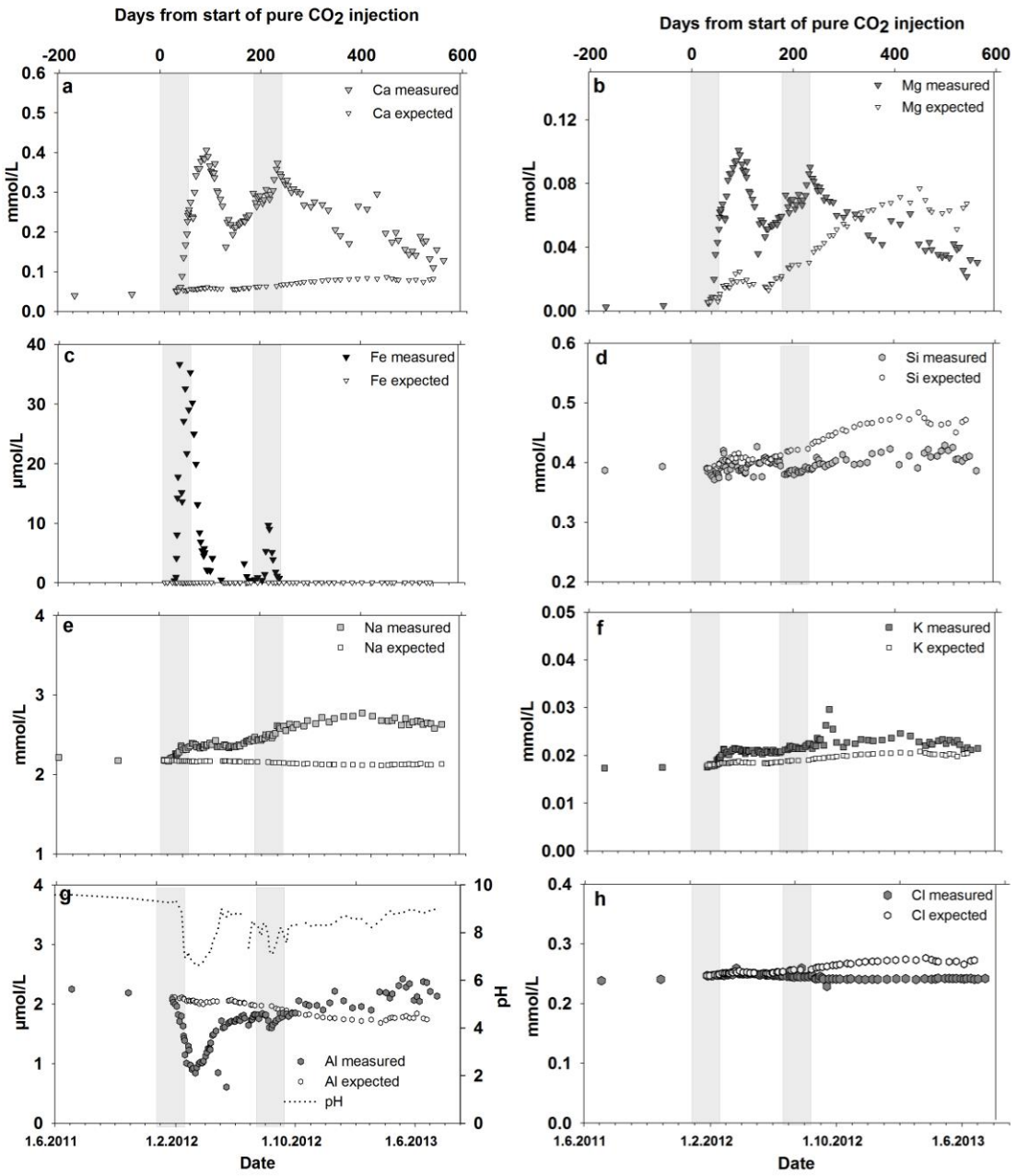

Figure 3. Concentrations of Ca, Mg, Fe, Si, Na, K, Al, Cl and F collected from monitoring well HN-04 prior to, during, and after the injection of CO_2 and CO_2/H_2S into the CarbFix Storage site. The timing of both gas injections is indicated by grey bars. Note the pH of the fluid samples is plotted together with the Al concentrations. The results of mass balance calculations depicting expected values for these concentrations, assuming pure mechanical mixing of the injected solution is also shown in these plots.

Figure 4. Photograph illustrating the presence of precipitates on the water sampling pump recovered from monitoring well HN-04 on the 13th of August 2013. The diameter of the pump is 101 mm.

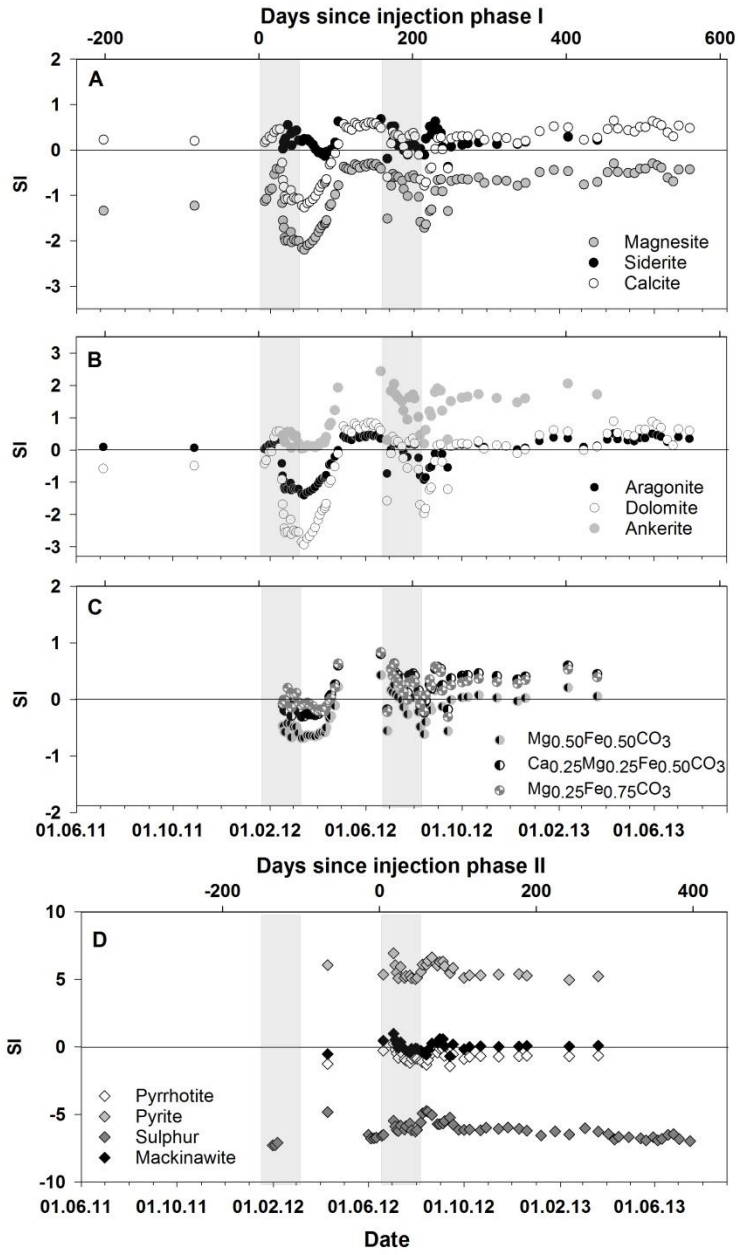

Figure 5. Saturation indices (SI) of collected HN-04 well water samples with respect to A) magnesite siderite and calcite; B) dolomite, aragonite and ankerite, C) Mg-Fe and Ca-Mg-Fe solid solutions, and D) pyrrhotite, pyrite, sulphur and mackinawite prior to, during, and after the injection of pure CO_2 and a CO_2/H_2S gas mixture into the CarbFix Storage site. All saturation indices were calculated assuming the oxygen fugacity was controlled by equilibrium of the H_2S/SO_4^{2-} as a redox couple. Note that positive, negative, and zero SI values correspond to aqueous fluids that are supersaturated, undersaturated, and at equilibrium with the indicated mineral. The timing of both gas injections is indicated by grey bars.

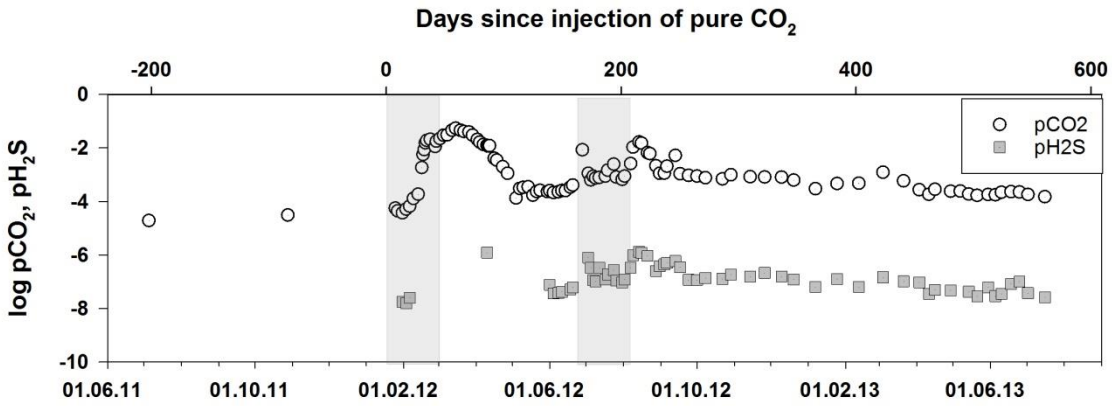

Figure 6. Partial pressures of CO_2 and H_2S prior to, during and after both injection experiments.

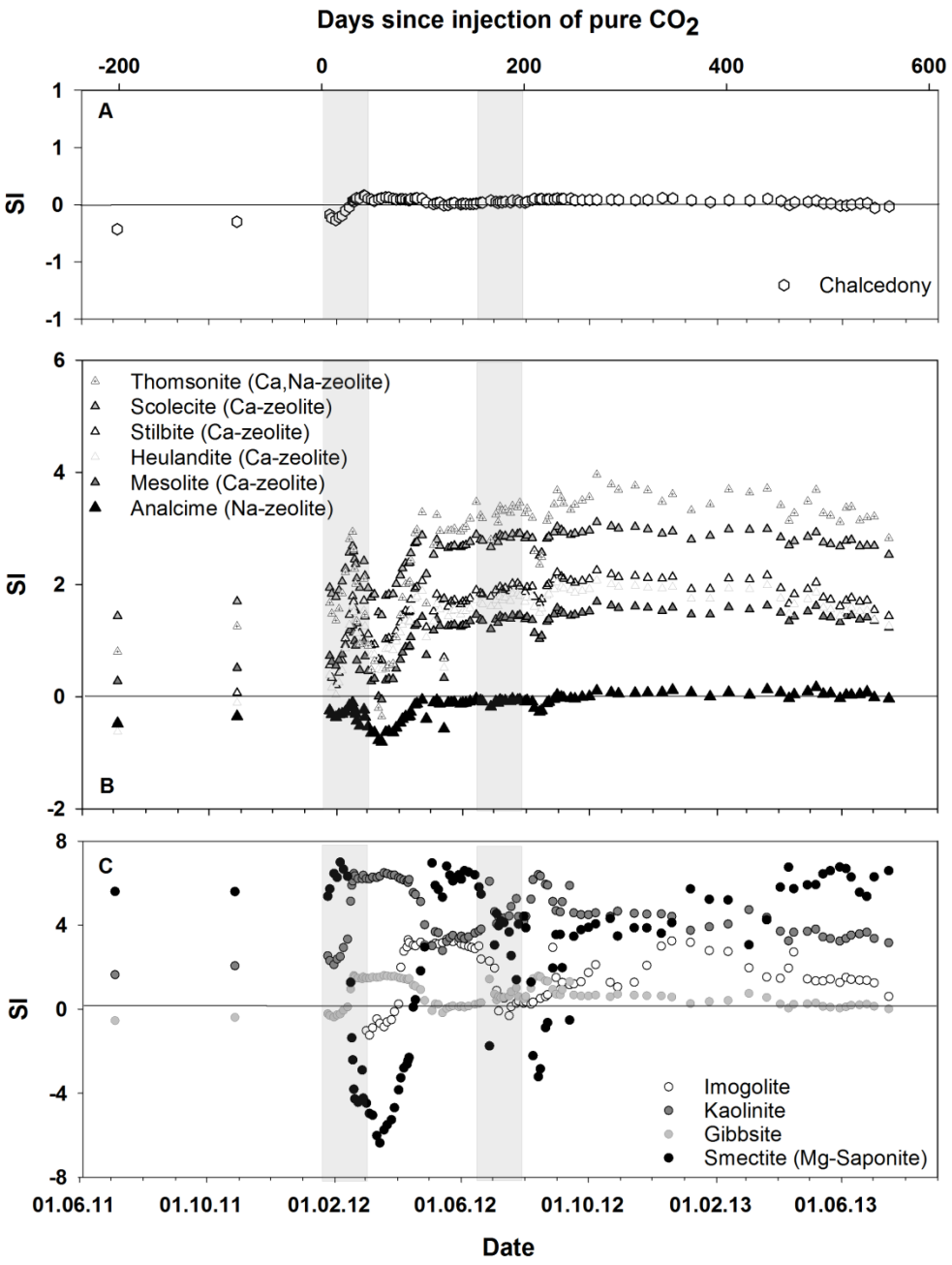

Figure 7. Saturation indices (SI) of collected HN-04 well water samples with respect to A) chalcedony, B) the zeolites previously identified in the area, and C) selected clay-minerals prior to, during, and after the injection of pure CO_2 and a CO_2/H_2S gas mixture into the CarbFix Storage site. Note that positive, negative, and zero SI values correspond to aqueous fluids that are supersaturated, undersaturated, and at equilibrium with the indicated mineral. The timing of both gas injections is indicated by grey bars.

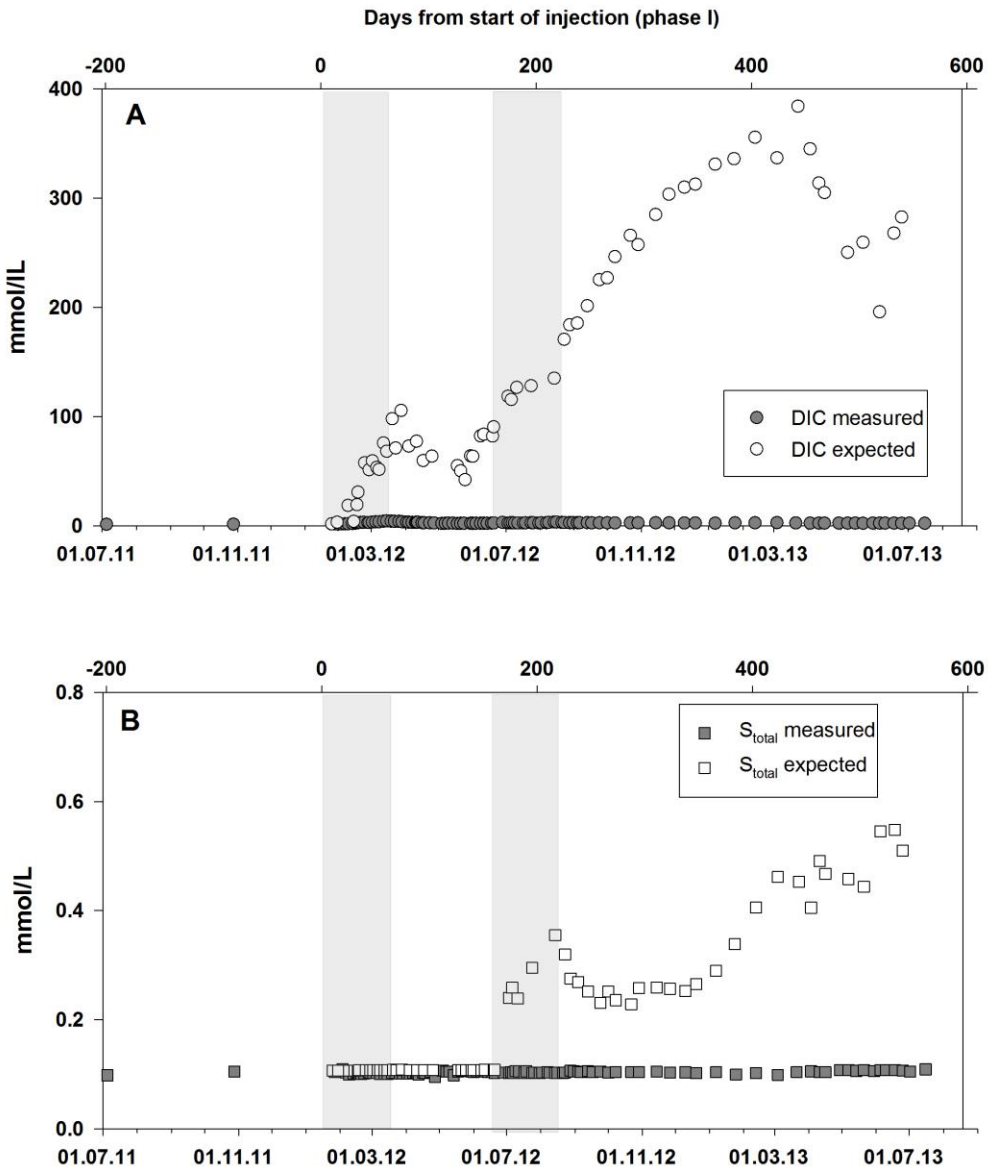

Figure 8. Comparison of measured and calculated non-reactive mixing concentrations of DIC and sulphur – see text. The timing of both gas injections is indicated by grey bars.

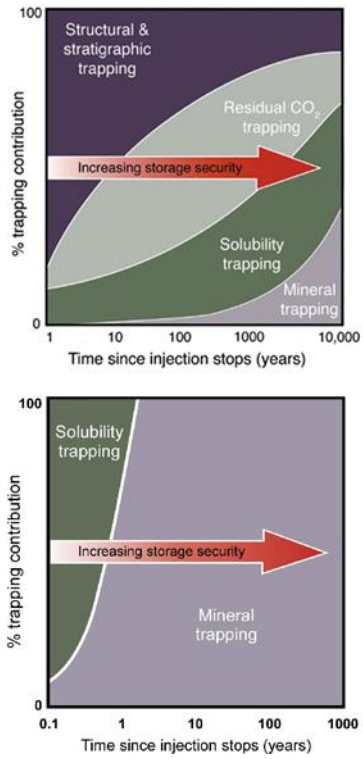

Figure 9. Schematic illustration of the contribution of various trapping mechanisms to the geologic storage as a function of time, a) injection of buoyant supercritical CO_2 into sedimentary rocks, modified from Benson et al. (2005), b) injection of CO_2 dissolved in water into basaltic rocks via the CarbFix method.